J. Fluid Mech. (1982), *vol.* 123, *pp.* 187–217
Printed in Great Britain

Turbulent Couette flow between concentric cylinders at large Taylor numbers

By G. P. SMITH
Trinity Hall, Cambridge

AND A. A. TOWNSEND
Emmanuel College, Cambridge

(Received 11 January 1982 and in revised form 10 May 1982)

Measurements have been made of the Couette flow in the annular space between concentric cylinders with a radius ratio of 1·5, the outer cylinder being held stationary and the inner one rotated at speeds to give Taylor numbers in the range $1{\cdot}0 \times 10^4$–$2{\cdot}3 \times 10^6$ times the critical value for first instability of the steady viscous flow. Mean velocities have been measured both with Pitot tubes and with linearized hot-wire anemometers, and turbulent intensities and stresses, frequency spectra and space–time correlations have been obtained using single hot-wire anemometers of X-form and linear arrays of eight single-wire anemometers. For Taylor-number ratios to the critical number less than 3×10^5, the most prominent feature of the flow is a system of toroidal eddies, encircling the inner cylinder and uniformly spaced in the axial direction with nearly the separation of the Taylor vortices of the viscous instability. They are superimposed on a background of irregular motion and, except within the thin wall layers, the toroidal eddies contribute more to the total intensity. With increase of rotation speed, the toroidal eddies lose their regularity, and they cannot be clearly distinguished at Taylor-number ratios beyond 5×10^5.

The change of flow type from quasi-regular toroidal to fully irregular turbulent takes place over an extensive range of Taylor-number ratio centred near 3×10^5, and it may be linked with changes in the thin wall layers that separate the flow boundaries from the central region of nearly constant circulation. For ratios over 5×10^5, an appreciable part of the wall layers is comparatively unaffected by flow curvature and has a logarithmic distribution of mean velocity similar to that found in channel flows. It is suggested that the motion in the wall layers changes from a set of Görtler vortices characteristic of curved-wall flow to the more irregular motion found on plane walls, causing the toroidal eddies to break into sections of length ranging from a considerable fraction of the flow perimeter to nearly the separation of the cylinders. Changes in the frequency spectra of the radial and azimuthal velocity fluctuations are consistent with such a change.

1. Introduction

In 1923, G. I. Taylor showed both by calculation and experiment that, above a critical speed, the steady viscous flow between concentric rotating cylinders is unstable to small axisymmetric disturbances if the ratio of flow circulation at the inner cylinder to that at the inner one is less than unity. For circulation ratios between zero and one, the instability leads first to the development of toroidal eddies encircling the inner cylinder and equally spaced in the axial direction, while, for negative ratios,

pairs of radially separated, contrarotating eddies form, the motion of the inner eddies much more intense than the outer ones. As the rotation speed increases, the toroidal eddies grow in strength before a series of transitions between multicellular modes with velocity varying periodically both in the azimuthal and axial directions (Coles 1965). The regularity of the motions and the complexity of transitions between modes has attracted much attention, and many papers have dealt with theoretical and experimental work (for a recent review see Di Prima & Swinney 1981).

Less is known about the irregular turbulent motions that succeed the cellular modes at large speeds of rotation. Three classes of flow might be distinguished, with characteristics that might be related either to the mechanism of transition or to the Rayleigh criterion for stability of curved flow. Flows with circulation ratios greater than one are stable to all small axisymmetric perturbations, and undergo catastrophic transition directly to turbulent motion at Reynolds numbers (based on flow width and velocity difference) considerably larger than that for plane Couette flow. For the flow with the inner cylinder stationary, the mean transmitted torque is only several times the calculated value for steady viscous flow, even for Reynolds numbers as high as 10^5 (Taylor 1936). The whole of the annular space is not filled with fluid in turbulent motion, which is confined to spiral bands embedded in nearly laminar flow (Van Atta 1966). If the cylinders rotate in opposite directions, transition to turbulent flow takes place at speeds above the critical speed for development of toroidal eddies, but the turbulent motion is weak, and, to judge from the *velocity profiles* of Wang & Gelhar (1970), the transmitted torque at Reynolds number of 10^5 is only several times the calculated viscous torque. In both these kinds of flow, the mean circulation increases radially outward over most of the annular region, and the Rayleigh criterion implies that the effects of flow curvature are stabilizing.

In flows with circulation ratios between zero and one, the gradient of circulation is everywhere destabilizing, and initial instability occurs at Reynolds numbers typically one-tenth of that for plane Couette flow. In the flow with the outer cylinder stationary, the multicellular modes persist to rotation speeds of about twenty times the critical speed, to be succeeded by irregular motion containing well-developed toroidal eddies similar to those of the initial instability (Gollub & Swinney 1975; Koschmieder 1979; Barcilon *et al.* 1979). Unlike the other two kinds of Couette flow, the torque is large compared with the calculated viscous torque, and the mean circulation is almost constant over most of the annular space, except within thin wall layers of rapidly varying circulation.

The work to be described set out to compare turbulent motion in strongly curved flows with that in essentially unidirectional mean flows in channels or in boundary layers on plane surfaces, and the axisymmetric Couette flow was selected as a well-defined example of curved flow. Since the object was to measure a wide range of flow quantities with hot-wire anemometers, the flow width and flow velocities chosen for experimental convenience dictated rotation speeds from one hundred to over one thousand times the critical speed for first instability. As it turned out, although the flow Reynolds numbers are large, considerable changes in the motion were observed as the rotation speed increased, and the reasons for them are of interest for the study of specifically Couette flow. A consequence is that some of the measurements are of flow structure and relevant to theoretical treatments such as those of Howard (1963) and Nickerson (1969), others are of local quantities such as Reynolds stress and turbulent intensity, which are used in current calculation methods for plane or weakly curved flow.

2. Notation

The flow is described using cylindrical polar coordinates r, θ, y, which are respectively the distance from the axis of rotation, the angular position and the displacement parallel to the axis. The corresponding components of flow velocity are w (in the direction of shear), $U+u$ (in the flow direction), and $V+v$ (parallel to the axis), where U and V are the mean velocities in the circumferential and axial directions, and should depend only on distance from the axis. The flow is essentially one of constant density, and stresses, torques and angular momenta are used in the kinematic forms, that is, as the mechanical values divided by the fluid density. Then

R_1, R_2 are the radii of the inner and outer cylinders;

U_1 is the peripheral velocity of the inner cylinder;

$Re = U_1(R_2-R_1)/\nu$ is the flow Reynolds number;

$T = \dfrac{2(1-\eta)}{1+\eta} Re^2$ is the flow Taylor number;

$\eta = R_1/R_2$ is the radius ratio ($\frac{2}{3}$ for the cylinders used);

$T_c = 2337$ is the critical Taylor number for instability of the laminar flow;†

$T^* = T/T_c$ is the Taylor-number ratio;

$-\tau_1$, τ_2 are the surface stresses exerted by the flow on the two cylinders;

$2\pi G = -2\pi\tau_1 R_1^2 = 2\pi\tau_2 R_2^2$ is the torque transmitted per unit length of cylinder;

$z = r-R_1$, is the distance from the inner cylinder;

$d = R_2-R_1$, is the gap between the cylinders;

$U^* = (U_1-U)/\tau_1^{\frac{1}{2}}$ in the wall layer on the inner cylinder, *or* $U/\tau_2^{\frac{1}{2}}$ in the layer on the outer cylinder;

$z^* = \tau_1^{\frac{1}{2}}(r-R_1)/\nu$ near the inner cylinder and $\tau_2^{\frac{1}{2}}(R_2-r)/\nu$ near the outer cylinder;

k, A are the constants for the logarithmic distribution of velocity in turbulent flow near a plane wall;

V_c is the axial convection velocity of the toroidal eddies;

$R_{ij}(\mathbf{r};\tau) = \overline{u_i(\mathbf{z}, t)\, u_j(\mathbf{z}+\mathbf{r}, t+\tau)}$ is the correlation function for velocity fluctuations at points separated by $\mathbf{r}$ in space and by τ in time;

$\phi_{ij}(\omega)$ is the frequency power spectrum of $\overline{u_i u_j}$;

$\omega^* = \omega R_1/U_1$ is a non-dimensional frequency ratio.

The subscripts i and j in the correlation and spectrum functions are 1 for u, the circumferential component, 2 for v, the axial component, and 3 for the radial component.

3. Experimental arrangements

The Couette flow is generated in the annular space between two concentric cylinders, the inner one of length 1·80 m and the outer of length 1·82 m. The inner cylinder, of diameter 305 mm, may be rotated about its axis of symmetry at rotational speeds up to 24 rev/s, with a peripheral speed of 23 m/s. The outer cylinder is stationary and has a nominal inside diameter of 457 mm, although in places its shape differs from the cylindrical by one or two millimetres. The measurements described were made over the speed range 1·5–24 rev/s, corresponding to flow Reynolds numbers from 7300 to 117 000, or Taylor numbers from $2{\cdot}1\times10^7$ to $5{\cdot}5\times10^9$. From the calculations of Roberts (1965), the critical Taylor number for a radius ratio

† The value of the critical Taylor number has been found by interpolation between values calculated by Roberts (1965).

of $\frac{2}{3}$ is 2337 (or a critical Reynolds number of 76·44), and the speed range covers Taylor numbers in ratios to the critical value from $0{\cdot}9 \times 10^4$ to $2{\cdot}3 \times 10^6$, or ratios of rotational speed to critical speed from 95 to 1530.

If the ends of the annular-flow space are closed, the velocity patterns of the toroidal eddies are stationary, and they do not cause variations in the outputs from stationary hot-wire anemometers. To avoid this difficulty, a slow axial flow was induced by having the ends of the flow space partially covered by dissimilar circular diaphragms mounted on the ends of the inner, rotating cylinder and extending to within a few centimetres of the outer cylinder. The dimensions of the diaphragms are not critical and their only noticeable effect on the flow is through the axial convection of the toroidal eddies past the anemometer. Typically, the eddy-convection velocity was of order 0·005 of the peripheral velocity of the inner cylinder, or about 1 % of the mean-flow velocity near the middle of the flow.

Several forms of hot-wire anemometer have been used, all made from Wollaston wire with etched sections of platinum wire, with diameter 2·5 μm and lengths about 1 mm. They were controlled by conventional constant-resistance circuits to operate at overheat ratios of 0·5–0·6, and the frequency response is thought to be uniform to at least 10 kHz. For the measurements of mean velocity and total turbulent intensity, the outputs were linearized by assuming that bridge voltages are related to flow velocity by

$$E^2 = a + bU_{\mathrm{e}}^{\frac{1}{2}} + cU_{\mathrm{e}}, \tag{3.1}$$

where E is the bridge voltage (proportional to current through the wire), and a, b, c are constant for a particular wire. Here

$$U_{\mathrm{e}}^2 = U^2[\cos^2(\theta-\phi) + \alpha \sin^2(\theta-\phi)], \tag{3.2}$$

where U is the flow velocity, θ is the angle of inclination of the flow to the wire support, and ϕ, α are constants for the wire.

Mean values, mean squares and covariances of the anemometer outputs were measured with a correlator that digitizes the outputs at regular intervals and accumulates sums, squares and products over set time intervals. Frequency spectra and space–time correlations were computed from digital recordings on magnetic tape. Any necessary amplification of the anemometer outputs was performed by amplifiers with a flat response from direct current to over 10 kHz.

4. Distributions of mean velocity and mean angular momentum

Careful measurements of mean velocity have been made over the annular space for peripheral velocities of the inner cylinder from 1·71 m/s to 9·8 m/s, for the most part with linearized hot-wires calibrated in a neighbouring small wind tunnel but also with small Pitot-static tubes. It was found that U/U_1, the ratio of mean-flow velocity to peripheral speed, was nearly independent of rotation rate at the position $z/d = (r-R_1)/(R_2-R_1) = 0{\cdot}581$, with the value of $0{\cdot}390 \pm 0{\cdot}001$. This reference position was later used for *in situ* calibration, and, necessarily, all the distributions of mean velocity or mean angular momentum intersect at that point.

Figure 1 shows distributions of the angular-momentum ratio Ur/U_1R_1 over the range of peripheral velocities used, for Taylor number ratios from $1{\cdot}29 \times 10^4$ to $4{\cdot}24 \times 10^5$. To make clear the features of the distributions, figure 1 (*a*) has the scale of momentum ratio expanded around 0·5, figure 1 (*b*) has the scale of gap ratio expanded around zero, and figure 1 (*c*) has the scale expanded around one. For gap ratios between 0·1 and 0·9, the angular-momentum ratio is close to 0·50 at all speeds,

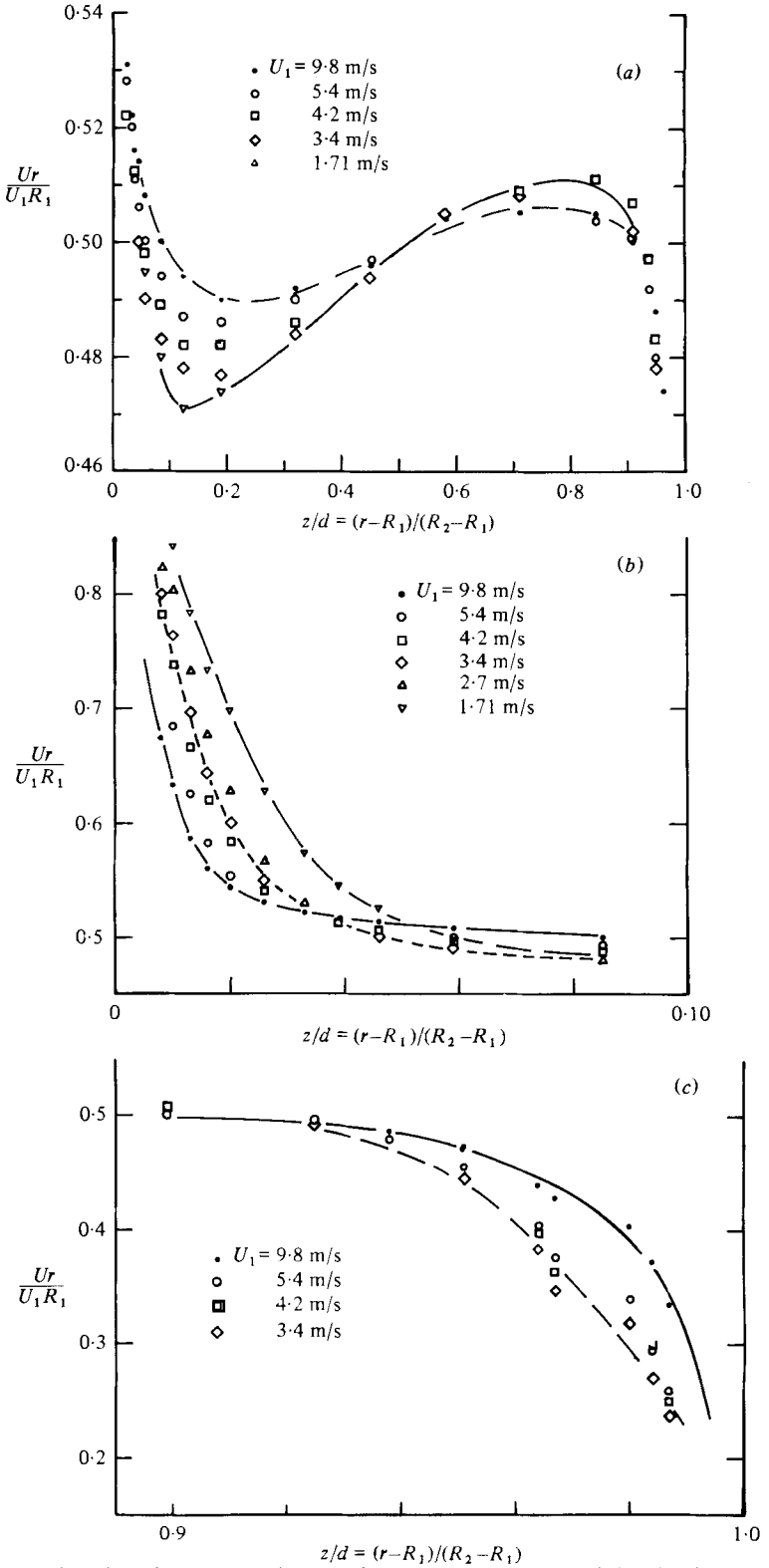

FIGURE 1. Radial distributions of the angular momentum ratio Ur/U_1R_1, for a range of rotation speeds: (*a*) over the central part of the flow; (*b*) near the inner, rotating cylinder; (*c*) near the outer, stationary cylinder.

although radial gradients of the ratio are definitely positive. Values of the non-dimensional gradient of angular momentum $U_1^{-1}\, d(Ur)/dr$ decrease systematically with increase of speed.

Almost all the variation of angular momentum occurs within the two wall layers, each of thickness no more than one-tenth of the flow width, and, since surface stresses are expected to be nearly proportional to the $\frac{7}{4}$ power of the rotation speed, their thicknesses become less at the higher speeds. A measure of the effects of flow curvature is the parameter,

$$\alpha = \frac{U/r}{dU/dr}, \tag{4.1}$$

the ratio of the angular velocity of the flow to the radial velocity gradient. In the central flow of nearly constant circulation, it is close to -1, indicating a dominance of curvature, but velocity gradients in the inner parts of the wall layers become relatively larger as the Reynolds number increases and then the inner wall flow may be little affected by the flow curvature.

The measurements have been replotted in non-dimensional forms appropriate to the dimensional consequences of making two extreme assumptions about the relative influences on the flow of curvature and velocity shear: (i) that curvature is so dominant that the analogy with natural convection in horizontally stratified fluids is valid, i.e. $|\alpha|$ is large everywhere except possibly deep within the viscous layers, and (ii) that there is a substantial region in each wall layer within which $|\alpha|$ is too small for flow curvature to have an appreciable effect. If curvature is dominant, the analogy with turbulent Bénard convection suggests that distributions of angular momentum near the inner cylinder are of the form,

$$U_1 R_1 - Ur = p_0 f(z/z_0), \tag{4.2}$$

where

$$p_0 = \frac{G^{\frac{3}{4}}}{(\nu U_1 R_1)^{\frac{1}{4}}}, \quad z_0 = \frac{R_1 \nu^{\frac{3}{4}}}{(G U_1 R_1)^{\frac{1}{4}}}$$

(see appendix). If curvature has no effect, the logarithmic universal wall distribution of velocity,

$$U_1 R_1 - Ur = \tau_1^{\frac{1}{2}}\, r\, g(\tau_1^{\frac{1}{2}} z/\nu), \tag{4.3}$$

should describe all the measurements deep within the wall layers.

Figure 2 shows velocity distributions in non-dimensional forms using the scales of angular momentum and length from (4.2) and (4.3). No points have been plotted for measurements outside the wall layer, i.e. beyond the distance for which the angular momentum first equals the central value of $\frac{1}{2}U_1 R_1$. The values of surface stress are derived from careful measurements of Reynolds stress made in the central flow for a peripheral speed $U_1 = 8{\cdot}0$ m/s, and a Reynolds number of 40640. The measurements, shown in figure 3, indicate an average value of the non-dimensional flux $G/(U_1 R_1)^2$ of $1{\cdot}10 \times 10^{-3}$, possibly accurate to 5%. Length and velocity scales for other speeds have been calculated by assuming the non-dimensional flux to vary either as $Re^{-\frac{1}{8}}$ (figure 2*a*) or as $Re^{-\frac{1}{4}}$ (figures 2*b*, *c*).

Comparing the three plots, the best collapse of data is achieved by using scales from (4.3), as if effects of flow curvature were negligible. In fact, a collapse in the viscous regions (z/z_0 less than 3 in figures 2(*a*, *b*), and z^* less than 10 in figure 2(*c*)) is assured by each choice of scales if correct values of transmitted torque have been used, and the radial range of appreciable variation of velocity outside the viscous regions is not large except at the higher speeds. For the three higher speeds and Reynolds numbers

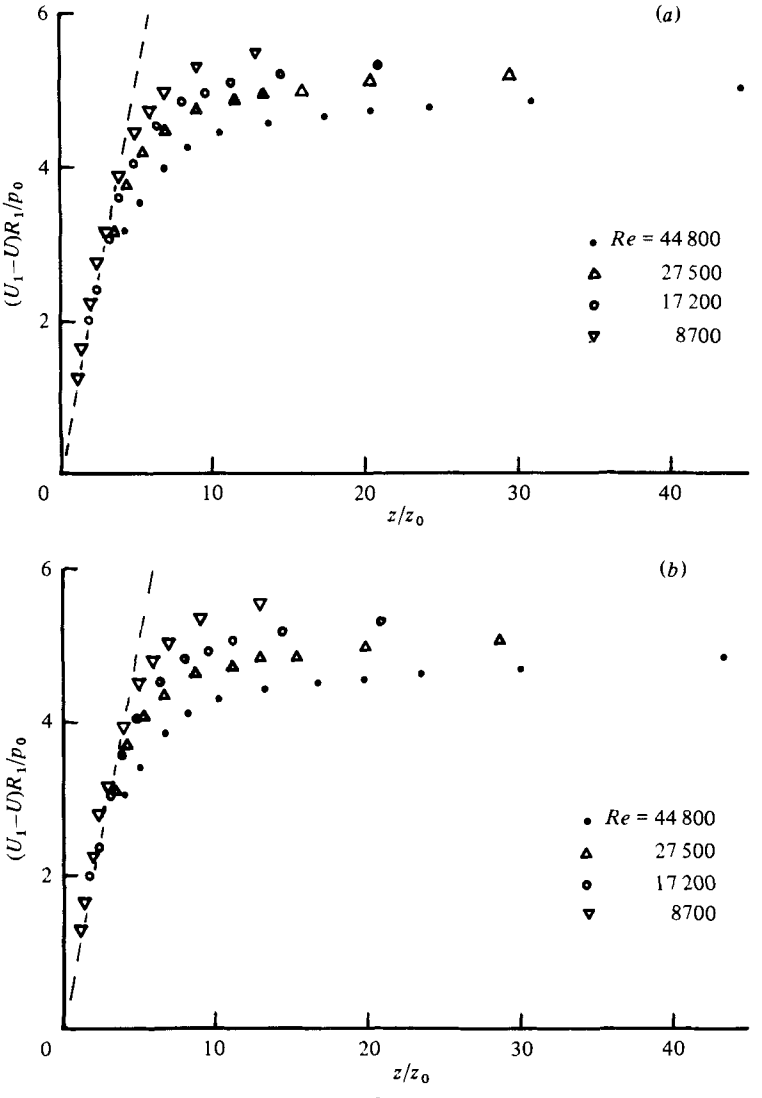

FIGURE 2(*a*, *b*). For caption see p. 195.

of $5{\cdot}0 \times 10^4$, $2{\cdot}8 \times 10^4$ and $2{\cdot}1 \times 10^4$, a plot of $(U_1 - U)/\tau_1^{\frac{1}{2}}$ against $\ln z^*$ (figure 2*d*) shows that the measured values lie nearly along a straight line

$$(U_1 - U)/\tau_1^{\frac{1}{2}} = k^{-1}(\ln z^* + A) \tag{4.4}$$

for values of z^* greater than thirty. The slope is consistent with a value of 0·41 for the Kármán constant k, but the additive constant A is about 1·8, a little less than the more usual value of 2·2.

Inspection of figures 2(*b*, *c*), which use convective scales, shows that departure from the linear variation in the viscous layer begins at successively larger values of non-dimensional distance as the Reynolds number decreases, indicating that flow curvature is not a dominant influence even at the lower speeds.

Measurements of velocity in the wall layer on the outer cylinder are more difficult, and positions of the hot-wire are not as accurate. Figures 2(*e*, *f*) are non-dimensional plots using the inertial scales $\tau_2^{\frac{1}{2}}$ for velocity and $\nu/\tau_2^{\frac{1}{2}}$ for length, and they show the

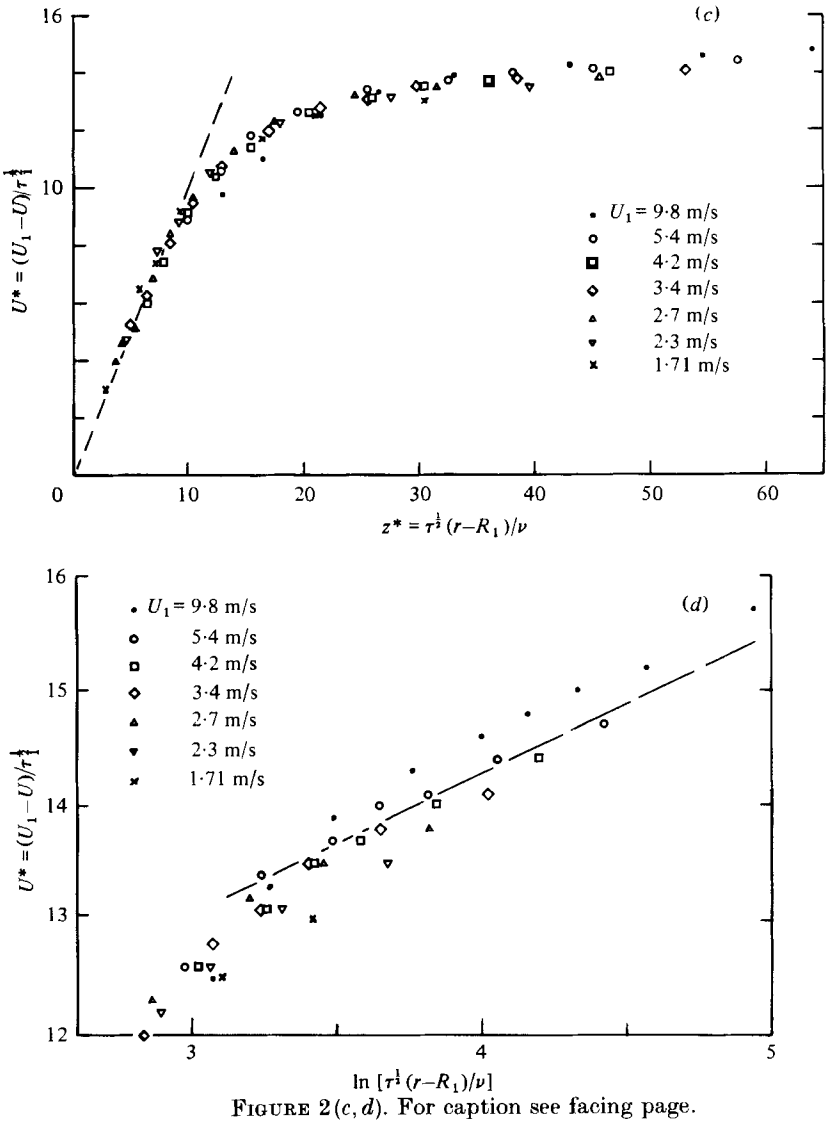

FIGURE 2(*c*, *d*). For caption see facing page.

measurements to be in fair agreement with the wall distribution (4.3) and, for values of z^* greater than thirty, with the logarithmic distribution (4.4).

Nakamura *et al.* (1981) have measured velocities near a cylinder rotating in essentially unbounded fluid, and they find that their results fit the distribution

$$U_1 - \frac{UR_1}{r} = \frac{\tau_1^{\frac{1}{2}}}{k}\left[\ln\frac{\tau_1^{\frac{1}{2}}(r^2 - R_1^2)\,R_1}{2\nu r^2} + A\right] \tag{4.5}$$

with $k = 0{\cdot}64$ and $A = 1{\cdot}8$. The measurements of figure 2(*d*) are for values of $(r - R_1)/R_1$ so small that the distributions (4.4) and (4.5) are not distinguishable.

5. The toroidal eddies

From visualization studies of the Couette flow in the range of Taylor-number ratio 400–10^5, Koschmieder (1979) and Barcilon *et al.* (1979) have shown that the greater

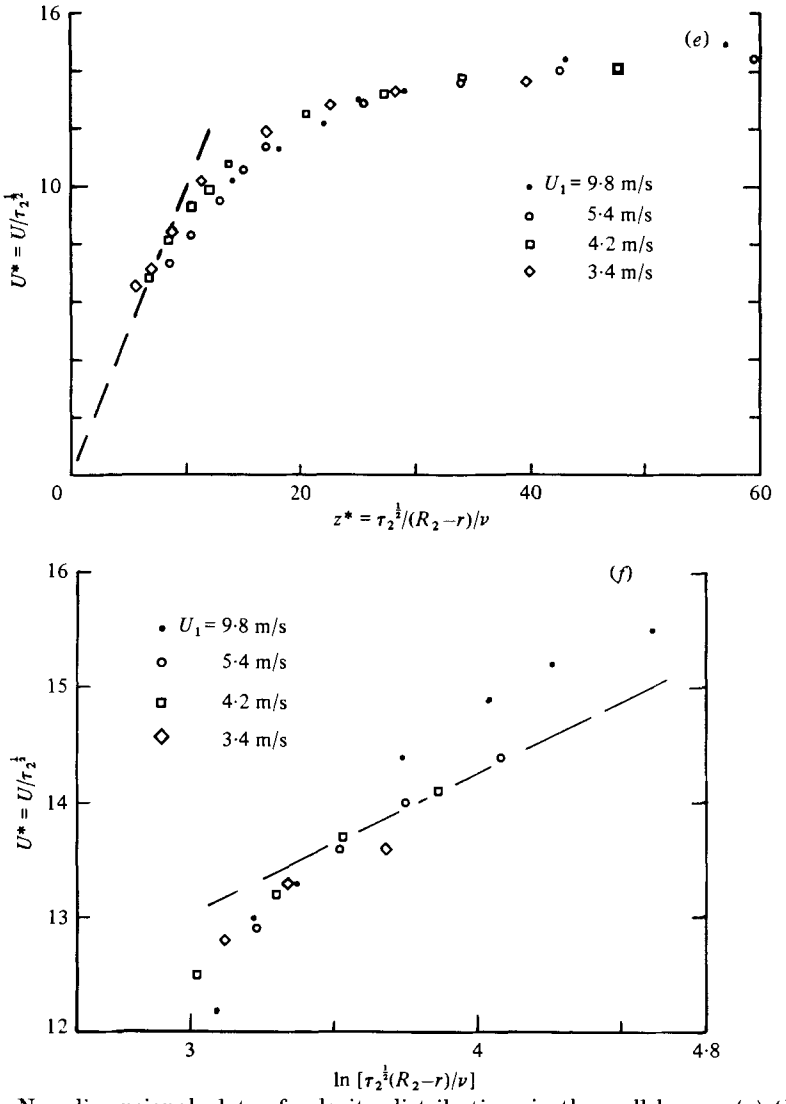

FIGURE 2. Non-dimensional plots of velocity distributions in the wall layers. (*a*) $(U_1-U)R_1/p_0$ versus $(r-R_1)/z_0$, assuming that $G/(U_1R_1)^2 \propto Re^{-\frac{1}{4}}$, i.e. convective scaling. (*b*) $(U_1-U)R_1/p_0$ versus $(r-R_1)/z_0$, assuming that $G/(U_1R_1)^2 \propto Re^{-\frac{1}{4}}$. (*c*) $U^* = (U_1-U)/\tau_1^{\frac{1}{2}}$ versus $z^* = \tau_1^{\frac{1}{2}}(r-R_1)/\nu$, assuming $G/(U_1R_1)^2 \propto \mathrm{Re}^{-\frac{1}{4}}$, i.e. inertial scaling. (*d*) U^* versus ln z^* for the inner wall layer. (*e*) $U^* = U/\tau_2^{\frac{1}{2}}$ versus $z^* = \tau_2^{\frac{1}{2}}(R_2-r)/\nu$ for the outer wall layer. (*f*) U^* versus ln z^* for the outer wall layer. (The straight lines on (*a*), (*b*), (*c*) and (*e*) have unit slope. The straight lines on (*d*) and (*f*) have slopes of k^{-1} with $k = 0{\cdot}41$.)

part of the motion is in the form of regularly spaced, toroidal eddies. If the annular space is sealed at both ends, the eddies are fixed in position and the flow patterns could be determined using a single sensor only by traversing in both the radial and axial directions. The toroidal eddies may be made to drift past a stationary anemometer by inducing an axial flow of magnitude small compared with flow velocities of the eddies. Then the anemometer output will oscillate with a passage frequency equal to the axial convection velocity divided by the wavelength of the eddy spacing. For typical measurements, the axial convection velocities were no more than 1 % of circumferential flow velocities, and even large flow patterns of dimensions

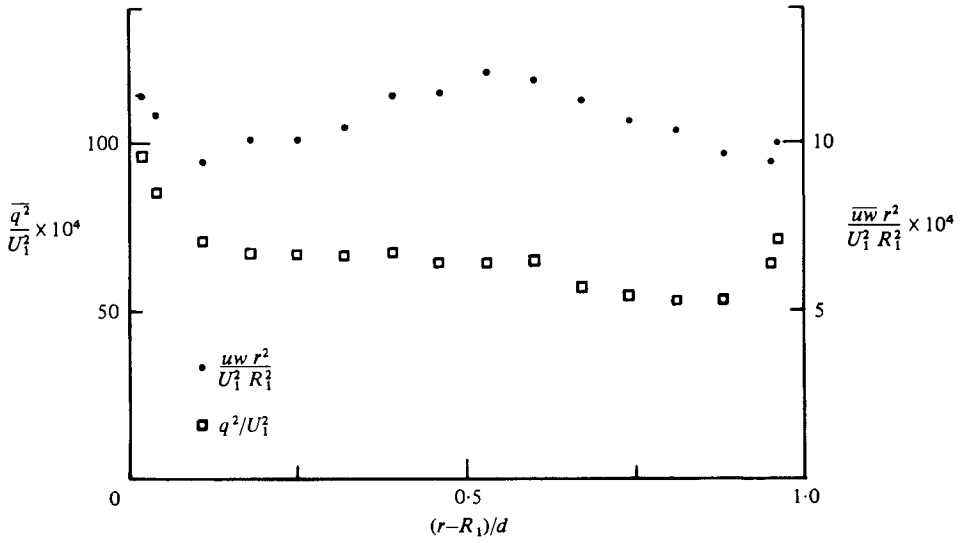

FIGURE 3. Radial distribution of the total radial flux of angular momentum expressed in the non-dimensional form $\overline{uw}r^2/(U_1 R_1)^2$, for a Reynolds number of 45600 ($T^* = 355000$).

comparable with the flow perimeter cause fluctuations of more than ten times the passage frequency as they are convected by at roughly the circumferential velocity.

The considerable difference in frequency between the contributions from the toroidal eddies and the non-axisymmetric irregular motion makes possible a clear separation. Figure 4 shows chart records of the output from a hot wire inclined to the mean flow at an angle of 45° in the diametral plane, after passage through a simple resistance–capacity filter to reduce contributions from frequencies above 5 Hz. For the smaller Taylor-number ratios (less than 2×10^5), the records show almost perfectly periodic fluctuations, but breaks and phase jumps become noticeable for ratios over 4×10^5 and periodicity is almost absent for ratios over 10^6. Figure 5 shows a series of chart records for a constant ratio of 9700 taken at various distances from the inner cylinder. The periodicity is good but the waveforms are far from sinusoidal, being peaked but symmetrical around the flow centre and asymmetric near the flow boundaries.

The degree of coherence of the oscillations may be assessed more precisely from measurements of the autocorrelations of the anemometer outputs. Figure 6 shows correlations for the radial component of the velocity fluctuation, at a fixed position $z/d = 0{\cdot}374$, for Taylor-number ratios of $0{\cdot}67 \times 10^5$, $4{\cdot}2 \times 10^5$, $8{\cdot}6 \times 10^5$ and $16{\cdot}5 \times 10^5$. For all but the shortest time delays, the autocorrelations can be represented very nearly by

$$R_{33}(\tau) = \overline{w(t)\, w(t+\tau)} = (A + Be^{-\tau/T_c}) \cos \omega_t \tau \qquad (5.1)$$

where ω_t is the (radian) frequency of passage, $A + B$ is the intensity of the toroidal eddies, B/A is a measure of the fluctuations of amplitude, and T_c is the coherence time. Values of the parameters are given in table 1.

A few digital recordings were made of the outputs from an array of eight single-wire anemometers, equally spaced along a line parallel to the axis of rotation with the sensitive elements at 45° to the mean flow in the yOr-plane. Figure 7 shows space–time correlations for pairs of wires with separations 0, 10, 60, 70 mm, and a peripheral cylinder velocity of $U_1 = 5{\cdot}24$ m/s or a Taylor-number ratio of $1{\cdot}11 \times 10^5$. Except for

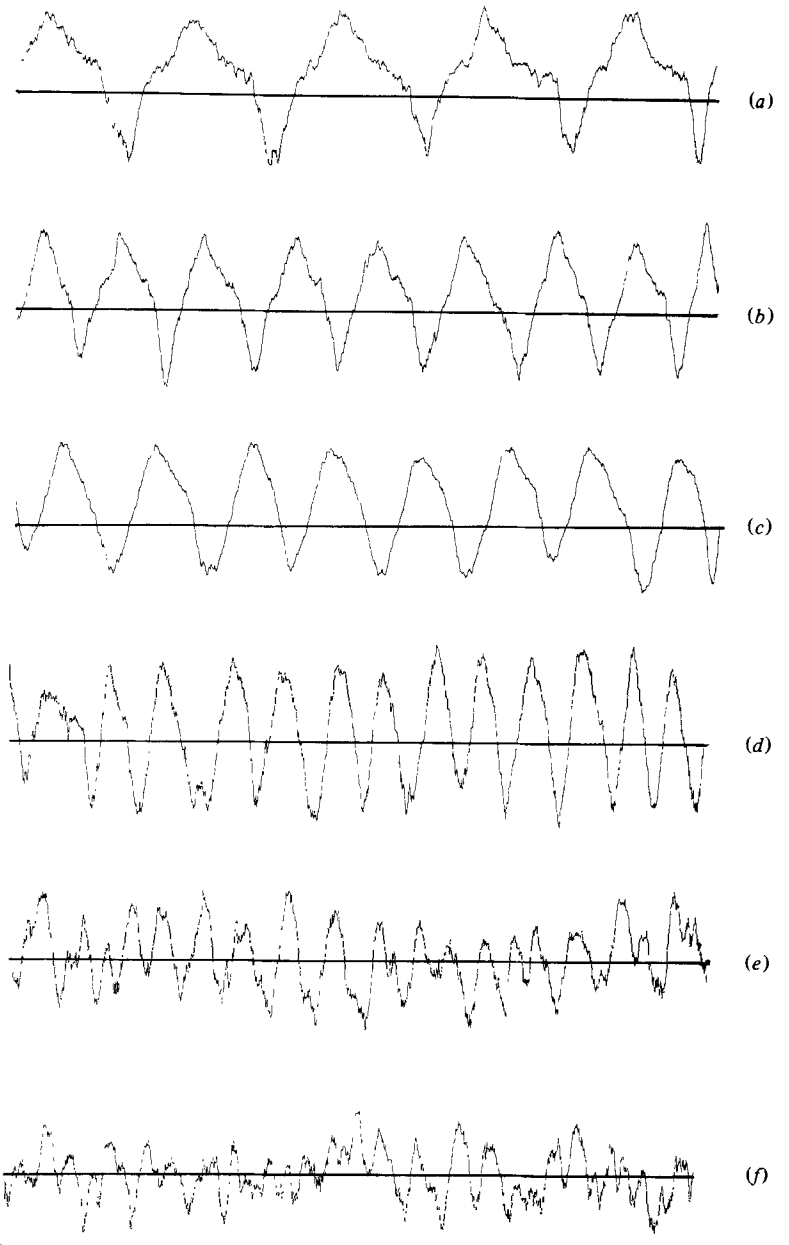

FIGURE 4. Chart records of the outputs from a hot-wire anemometer responding nearly to fluctuations of $u+w$, placed at $z/d = 0{\cdot}375$ near the flow centre: (*a*) $Re = 7800$, $T^* = 10400$, record duration 150 s; (*b*) 11800, 23800, 150 s; (*c*) 20200, 70000, 75 s; (*d*) 36200, 224000, 75 s; (*e*) 51500, 454000, 75 s; (*f*) 69000, 815000, 75 s.

a change of phase, the correlations between separated wires are very nearly those for a single wire. The phase change increases with spatial separation in the way expected from axial convection of a periodic flow pattern at a velocity of 30 mm/s. For sensor separation of 70 mm, the phase shift is nearly 180°, indicating a wavelength of 140 mm, in a ratio of 1·9 to the cylinder separation.

For the smaller rotation rates, the regularity of the oscillations is sufficient to be synchronized with a phase-locked loop oscillator, and passage frequencies determined

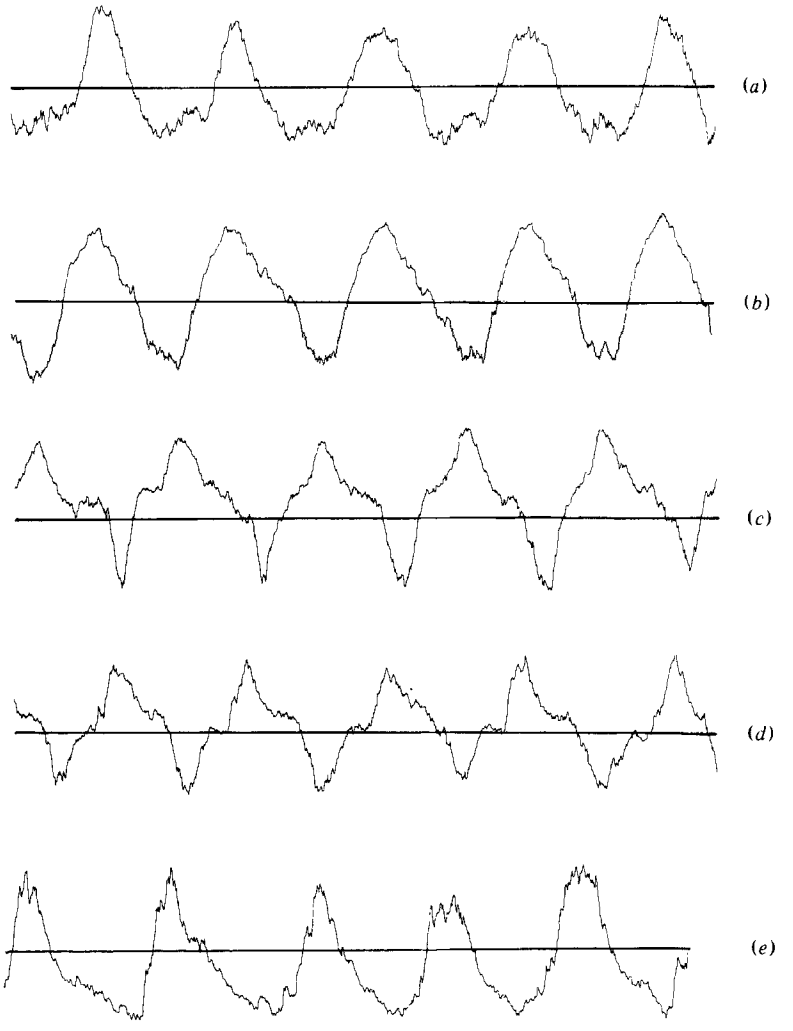

FIGURE 5. Chart records of the outputs from a hot-wire anemometer responding nearly to fluctuations of $u+w$, for a Reynolds number $Re = 7540$, $T^* = 9700$: (*a*) at $z/d = 0{\cdot}045$; (*b*) 0·12; (*c*) 0·375; (*d*) 0·635; (*e*) 0·895. Length of records 150 s.

in this way are shown in figure 8, together with frequencies from the autocorrelations. The passage frequencies are nearly proportional to peripheral speed, and, supposing the axial convection velocity to remain a constant fraction of that speed, the eddy spacing is almost independent of Taylor number.

6. Intensities of the toroidal and irregular motions

The toroidal eddies have axisymmetric flow patterns, which are convected axially past a fixed sensor with convection velocities around 0·004 U_1. On the other hand, flow patterns with variation in the flow direction will be convected around the inner cylinder with velocities comparable to the peripheral speeds of flow, around 0·4 U_1, and the consequent fluctuations are of frequencies much higher than those produced by the toroidal eddies. The difference is so large that the respective mean-square fluctuations may be easily determined by use of simple low-pass filters.

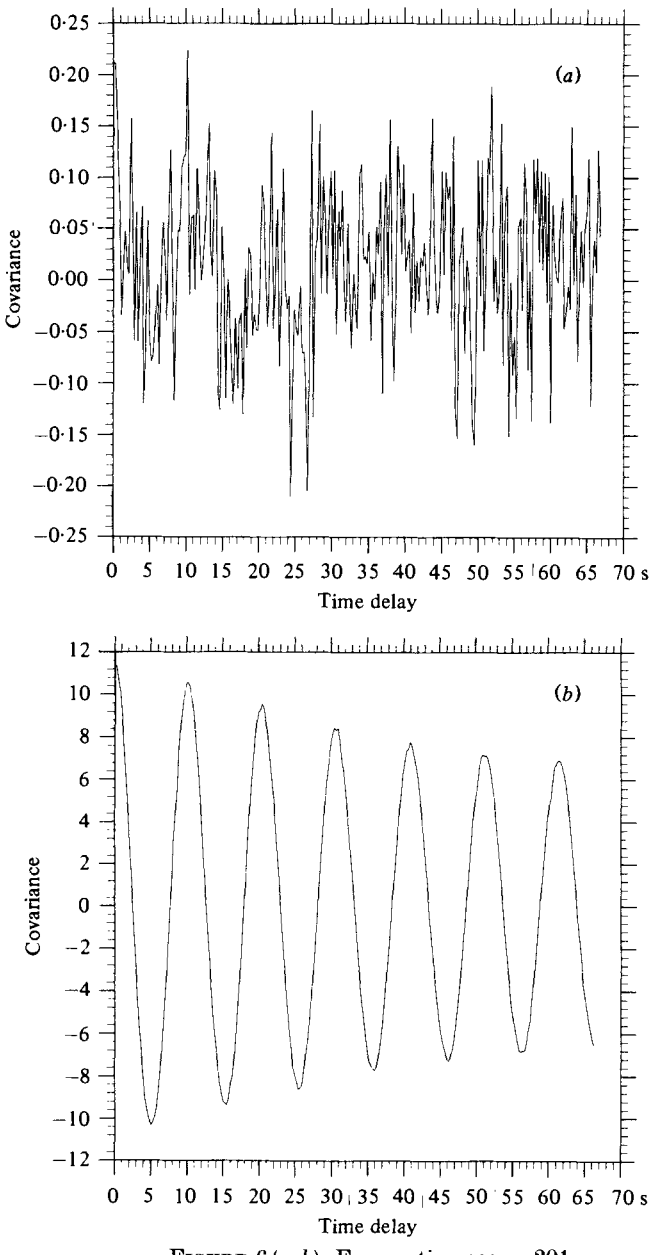

FIGURE 6(*a*, *b*). For caption see p. 201.

Assuming the spectrum of the irregular non-axisymmetric motion to be nearly independent of frequency over the pass band of the resistance–capacity filter, the mean square of fluctuations after passage through the filter is

$$I(\tau) = \frac{Q_t}{1+\omega_t^2\tau^2} + \frac{S}{\omega_t \tau}, \tag{6.1}$$

where τ is the time constant of the filter, Q_t is the mean square of fluctuations of the toroidal component, $\omega_t/2\pi$ is the frequency of passage, and S/ω_t is the spectral intensity of the irregular component at low frequencies.

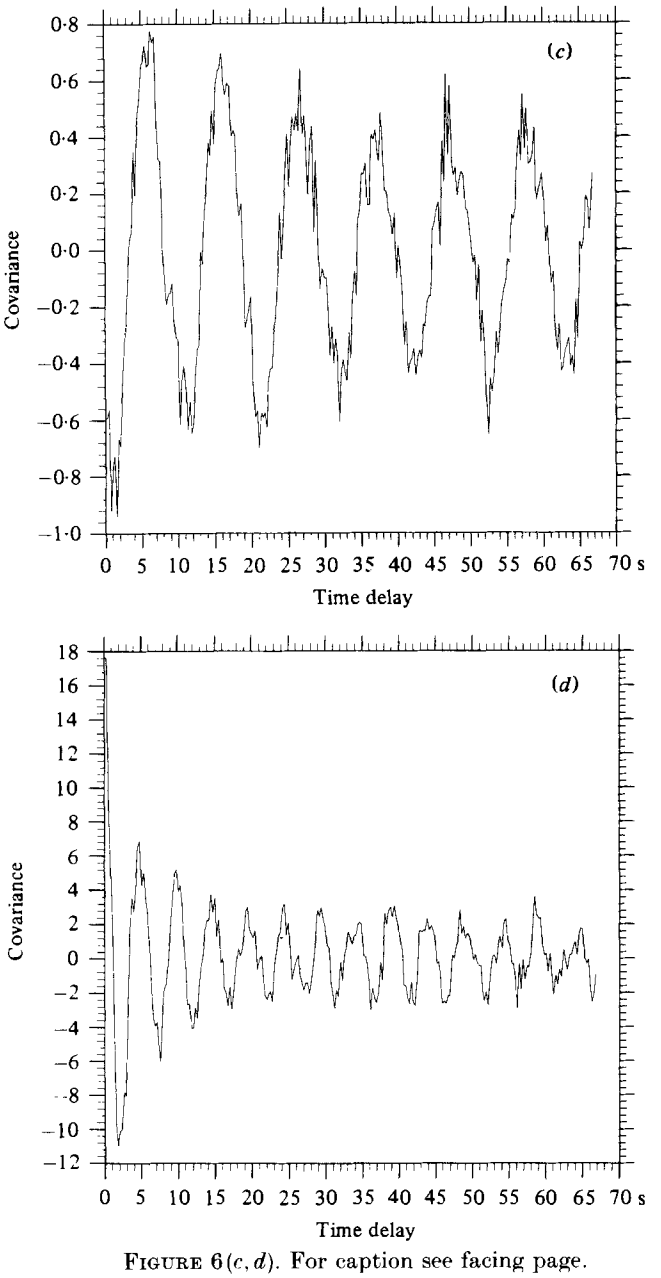

FIGURE 6(*c*, *d*). For caption see facing page.

The results shown in figures 9 and 10 have been obtained by measuring variances and covariances of the outputs from X-wires, before and after passage through filters of three different time constants, typically 0·1 s, 0·22 s and 0·47 s. Passage frequencies were found either from the output of a phase-locked oscillator or, for the higher rotation speeds, from an extrapolation of the frequency–speed plot (figure 8), and then values of Q_t and S were selected for best fit to the three equations of the form (6.1). Although the waveforms of the toroidal variations are noticeably non-sinusoidal (figure 5), the intensities of the harmonics are less than 5 % of the total and may be

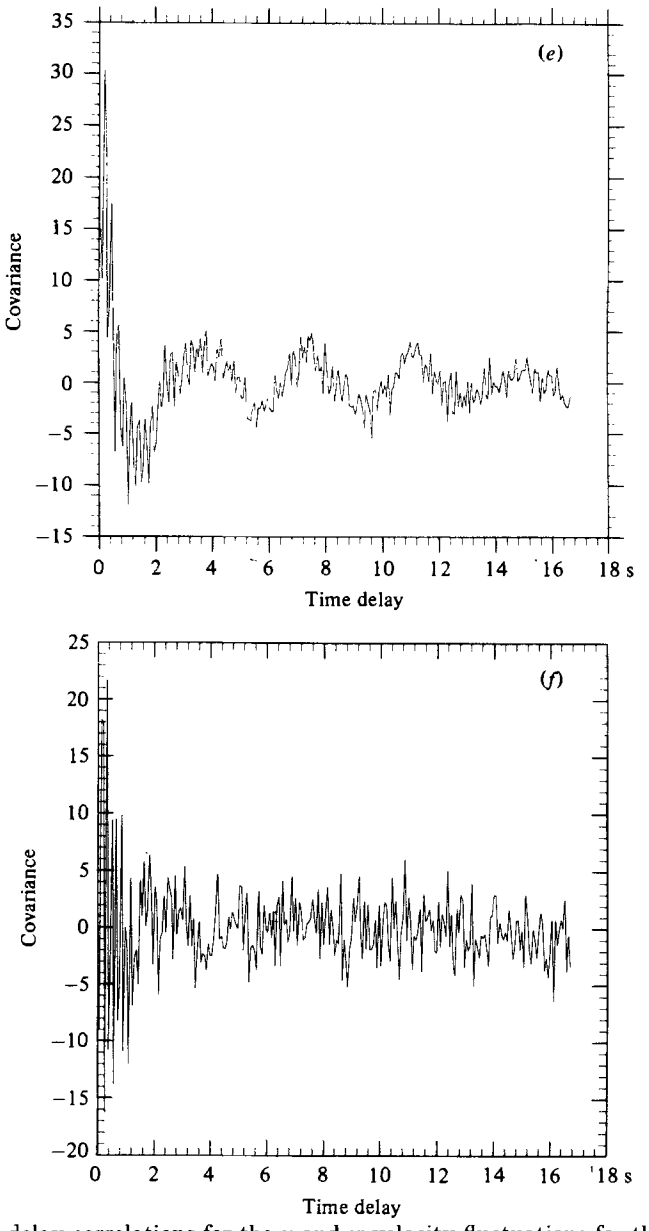

FIGURE 6. Time-delay correlations for the u and w velocity fluctuations for three rotation speeds at the position $z/d = 0{\cdot}635$. (*a*) $R_{11}(\tau)$, (*b*) $R_{33}(\tau)$, (*c*) $R_{13}(\tau)$ all for $Re = 20900$, $T^* = 70000$. (*d*) $R_{33}(\tau)$ for $Re = 51500$, $T^* = 454000$. (*e*) $R_{33}(\tau)$ for $Re = 74000$, $T^* = 940000$. (*f*) $R_{33}(\tau)$ for $Re = 103000$, $T^* = 1820000$. Units of the vertical scales are the same for (*a–c*), $Re = 20900$, but have not been normalized. Values of $\overline{w^2} = R_{33}(0)$ in the units are: (*a*)–(*c*) 19·6, (*d*) 83, (*e*) 197, (*f*) 221.

neglected. Intensities of the irregular component were found by subtracting values of Q_t from intensities measured without the filters.

The main features of the intensity distributions are as follows.

(*a*) *Toroidal eddies*

(i) Non-dimensional intensities of the axial component $\overline{v_t^2}/U_1^2$ are small near the flow centre and reach maximum values within the wall layers.

Re	T^*	$A/\overline{w^2}$	$B/\overline{w^2}$	$T_c U_1/R_1$	ωT_c	$\overline{w_t^2}/\overline{w^2}$
20900	74800	0·34	0·25	700	16·0	0·59
51500	454000	0·028	0·185	390	7·3	0·21
74000	940000	0·010	0·066	140	3·5	0·076
103000	1820000	0·003	0·029	170	3·5	0·032

TABLE 1. Coherence of the low-frequency oscillations of radial velocity. The quantities A, B and T_c are those used in (5.1). If the initial decrease of autocorrelation arises entirely from variation of amplitude with no variation of phase, A is the square of the mean amplitude and B is the mean square of the deviation of the amplitude from its mean value $A^{\frac{1}{2}}$.

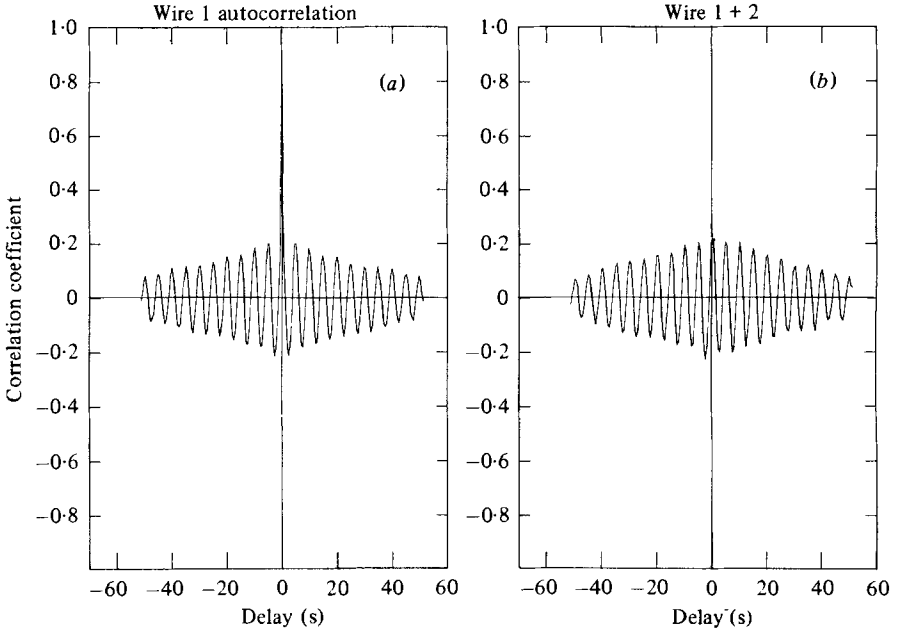

FIGURE 7 (a, b). For caption see facing page.

(ii) Intensities of the radial component $\overline{w_t^2}/U_1^2$ are small near the walls and reach maximum values near the flow centre.

(iii) Circumferential (streamwise) intensities $\overline{u_t^2}/U_1^2$, are much smaller.

(*b*) *The irregular motion*

(i) Axial intensities $\overline{v_r^2}/U_1^2$ and circumferential intensities $\overline{u_r^2}/U_1^2$ have their minimum values near the flow centre.

(ii) Radial intensities $\overline{w_r^2}/U_1^2$, reach maximum values near the flow centre.

(iii) Near the flow centre, radial intensities exceed axial intensities, and axial intensities exceed circumferential (streamwise) intensities. The sequence of relative values is the reverse of that found in unidirectional shear flows.

With increase of rotation speed, the relative intensity of the toroidal motion falls off sharply. Figure 11 shows ratios of the toroidal intensity $\overline{w_t^2}$ to the total intensity at a position near the flow centre for a range of rotation speeds. For Reynolds numbers less than 2×10^4 (Taylor-number ratios less than 7×10^5), the intensity of the toroidal component is greater than that of the irregular motion, but the intensity ratio decreases rapidly with increased speed and is around 0·05 for a Reynolds number of 10^5 or a Taylor-number ratio of $1{\cdot}5 \times 10^6$.

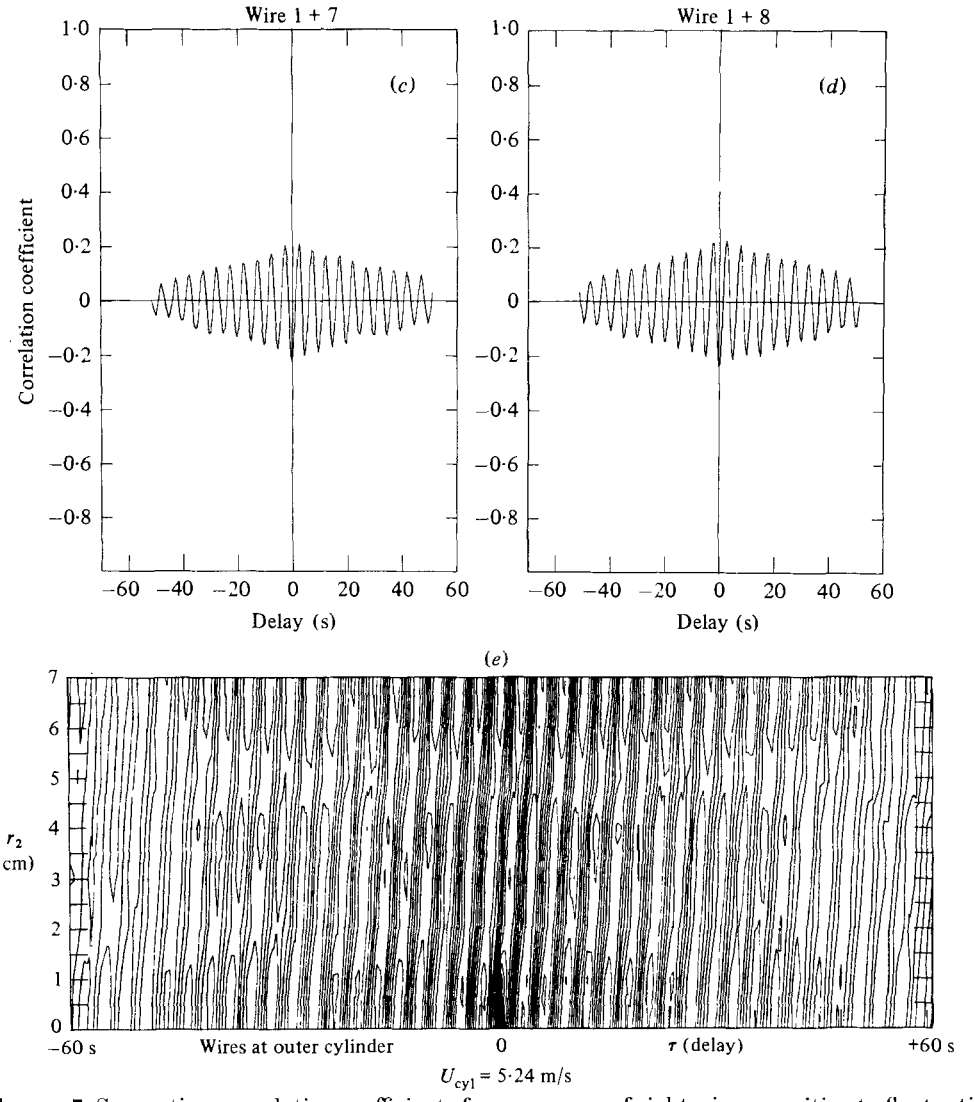

FIGURE 7. Space–time correlation coefficients from an array of eight wires, sensitive to fluctuations of $u+v$ and placed in a line parallel to the cylinder axis and close to the outer cylinder. (Re = 26600, T^* = 121000.) (*a*) autocorrelation for wire 1. (*b*) Correlation for wires separated by 10 mm. (*c*) Correlation for wires separated by 60 mm. (*d*) Correlation for wires separated by 70 mm. (*e*) Contours of equal correlation coefficient between an end wire and the other seven.

7. Frequency spectra of the irregular motion

From digital recordings of the outputs from X-wire anemometers, frequency spectra of the three velocity components have been calculated for ranges of frequency either 2–2000 Hz or 0·5–500 Hz and not including the passage frequency of the toroidal eddies. Several spectra are shown in figure 12, plotted as products $\omega\phi(\omega)$ of frequency and spectral intensity, against logarithmic scales of the non-dimensional frequency $\omega^* = \omega R_1/U_1$, the ratio of frequency to rotation rate of the inner cylinder. With this presentation, areas under the spectral curve remain proportional to contributions to total intensity from the particular range of frequency, and spectra of motions composed from eddies of similar size appear as peaked distributions with the maxima at frequencies comparable to the reciprocal of the average duration of

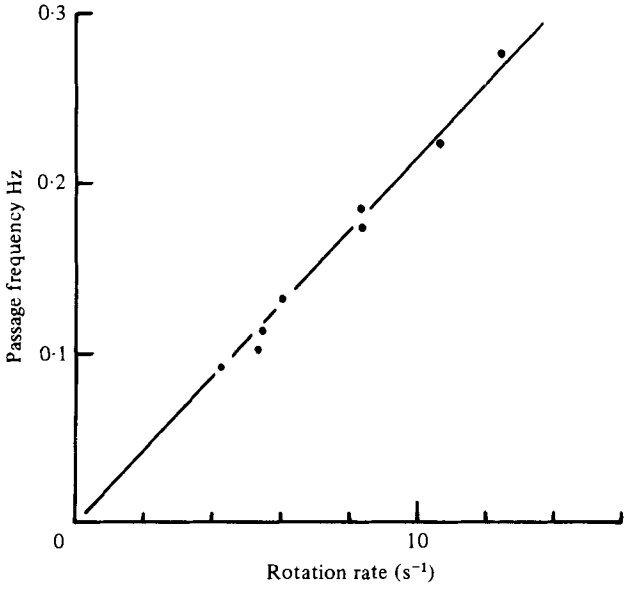

FIGURE 8. Passage frequency of the toroidal eddies as a function of cylinder rotation speed.

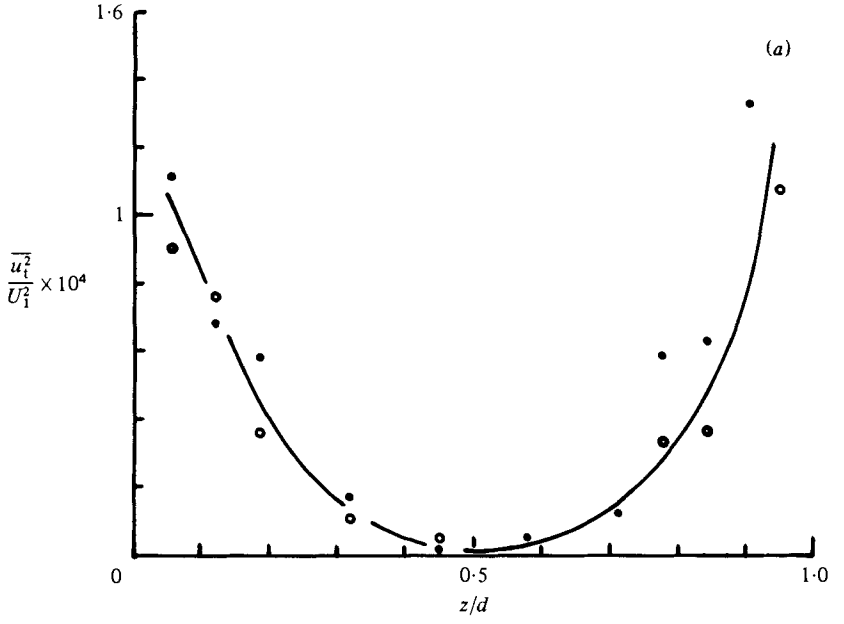

FIGURE 9(a). For caption see facing page.

eddy passage. For example, the spectra of many free turbulent flows resemble in form, $\phi(\omega) = (1+\omega^2)^{-1}$, for which the product $\omega\phi$ has a maximum value of 0·5 for $\omega = 1$, decreasing to one-half of that value for the frequencies ω_1, $\omega_2 = 2 \pm \sqrt{3}$, whose ratio is 13·9:1.

Compared with spectra of free turbulent flows, the measured spectra are very broad, with ratios of the half-intensity frequencies in the range 30–100, indicating that the fluctuations are composed of elements with an exceptionally wide range of durations contributing to the total intensity. Table 2 lists half-intensity frequencies and their

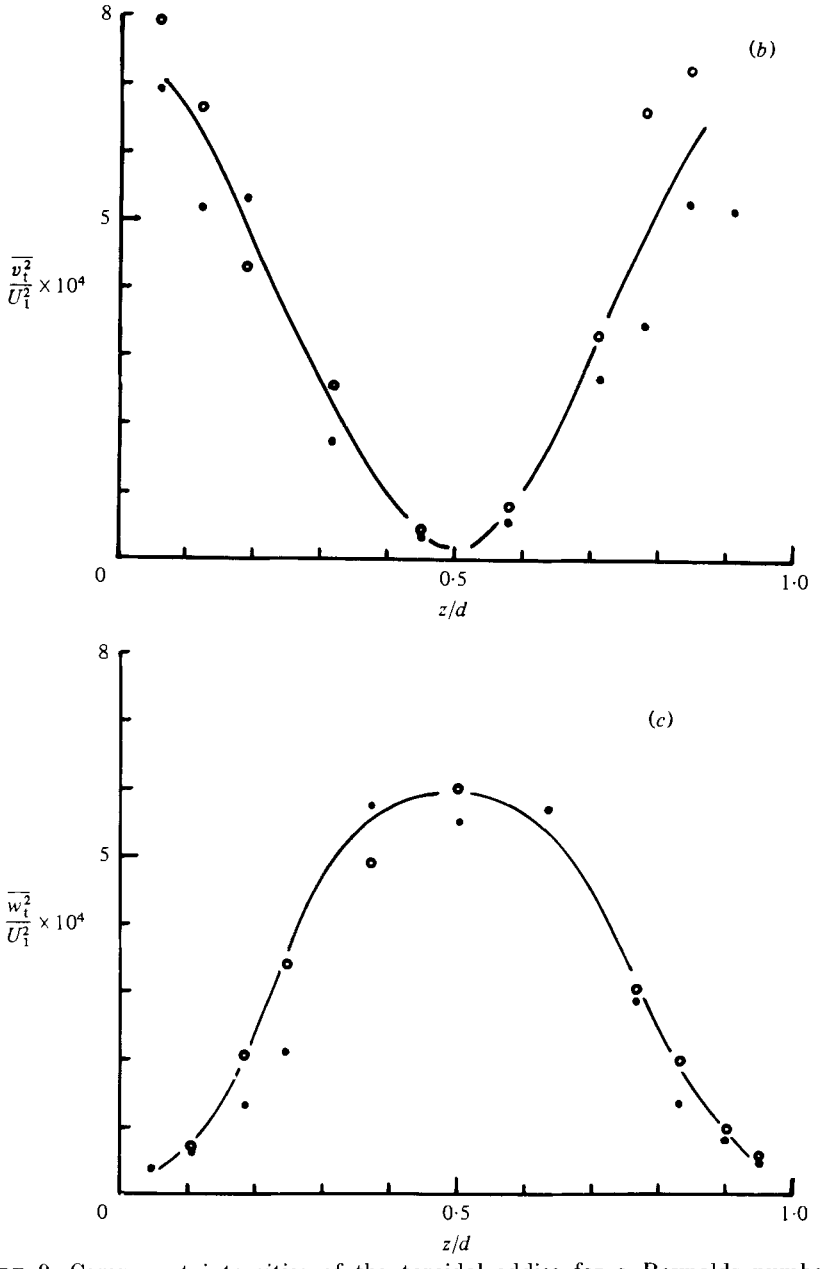

FIGURE 9. Component intensities of the toroidal eddies for a Reynolds number $Re = 51600$ ($T^* = 455000$).

ratios for four positions in the flow and for Reynolds numbers of $2{\cdot}1 \times 10^4$, $5{\cdot}2 \times 10^4$ and $9{\cdot}8 \times 10^4$ (Taylor-number ratios of $0{\cdot}75 \times 10^5$, $0{\cdot}46 \times 10^6$ and $1{\cdot}62 \times 10^6$). All the ratios are considerably larger than the values in typical free turbulent flows, but they are much larger at the two higher speeds than at the lowest speed.

If the fluctuations are composed of randomly occurring patterns of similar forms but variable duration, say $af[(t-t_0)/T]$, where a is an amplitude and T a measure of the duration, the contribution to the spectrum from patterns of a single duration is $QT\Psi(\omega T)$, where Q is the total contribution, and $\Psi(\omega T)$ is the power spectrum of

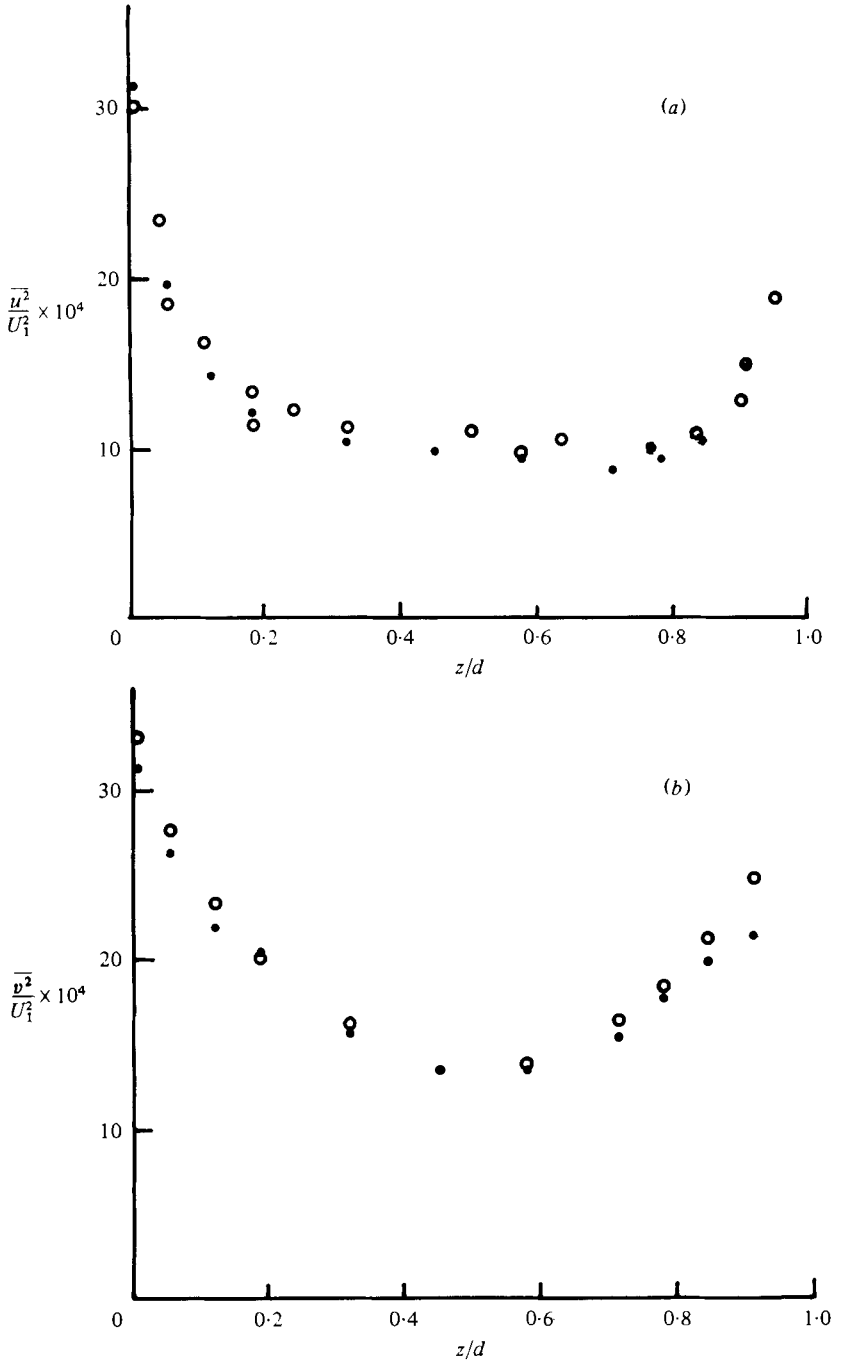

FIGURE 10(*a*, *b*). For caption see facing page.

the pattern, normalized so that $\int_0^\infty \Psi(x)\,dx = 1$. With a continuous range of durations, the total spectrum is the sum of contributions from all durations, i.e.

$$\phi(\omega) = \int_0^\infty Q(T)\,T\,\Psi(\omega T)\,dT, \tag{7.1}$$

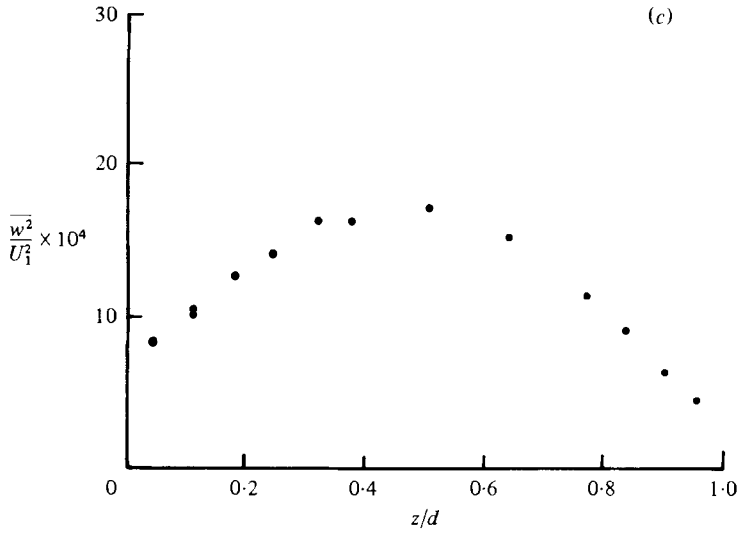

FIGURE 10. Component intensities of the complete motion for a Reynolds number $Re = 51\,600$ ($T^* = 455000$).

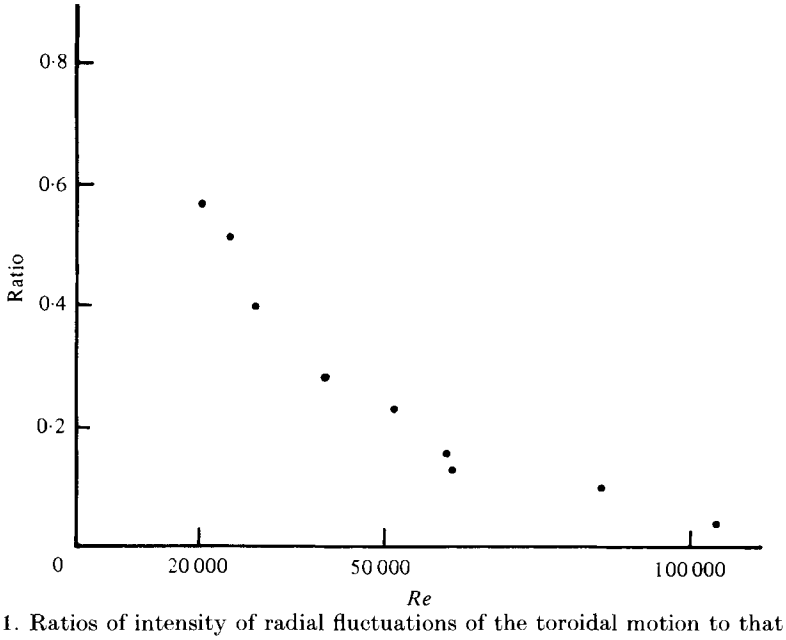

FIGURE 11. Ratios of intensity of radial fluctuations of the toroidal motion to that of the whole motion, for a range of Reynolds numbers and in the central flow ($z/d = 0{\cdot}50$).

where $Q(T)\,dT$ is the contribution to the intensity from components with durations from T to $T+dT$. Using the logarithmic plotting of figure 12, it is appropriate to use a distribution function $P(T) = TQ(T)$ specifying contributions from equal logarithmic ranges of duration, and then

$$\omega\phi(\omega) = \int_{-\infty}^{\infty} P(\ln T)\,\Phi(\ln T + \ln \omega)\,d(\ln T), \tag{7.2}$$

where $\Phi(x) = x\Psi(x)$ is the spectrum of a single component on the logarithmic scale of frequency.

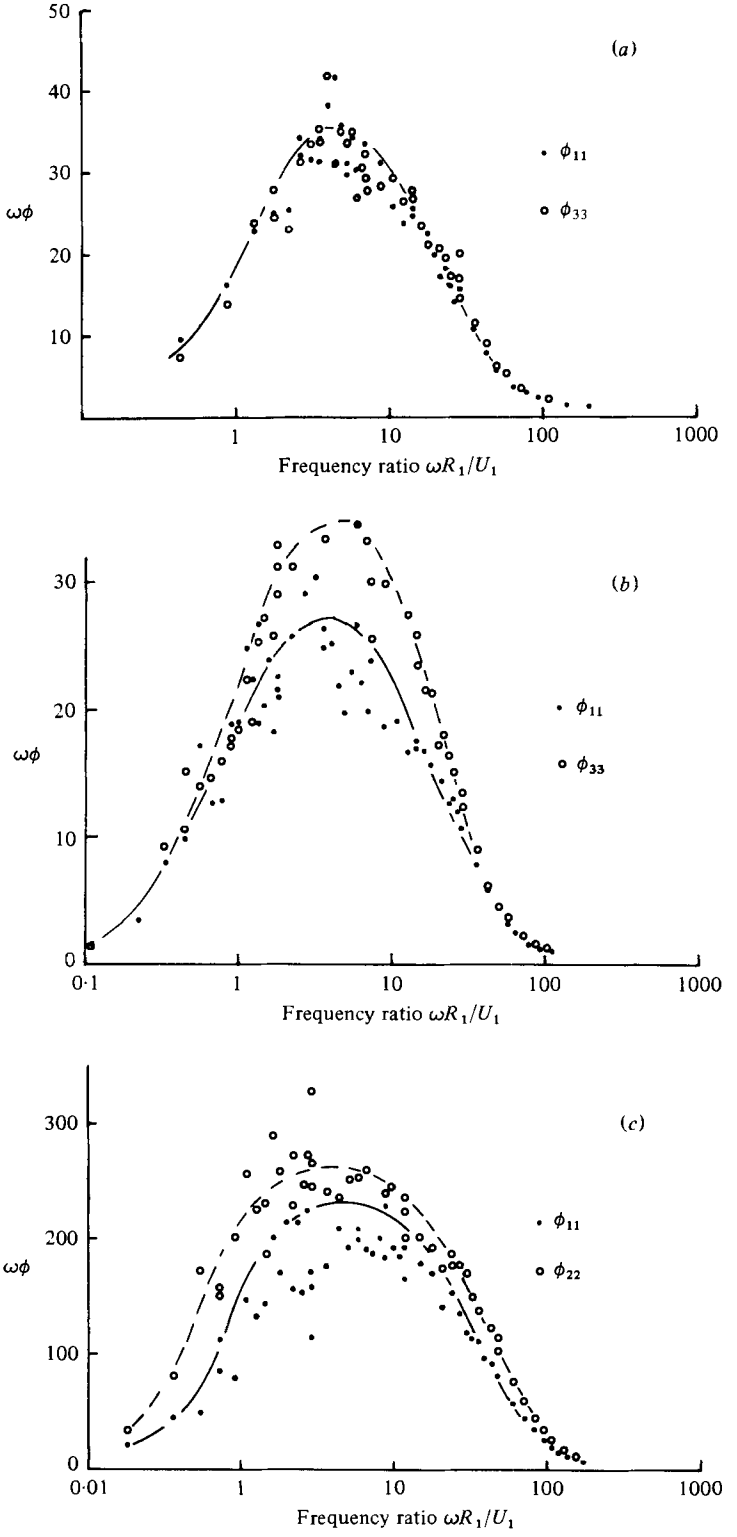

FIGURE 12(a, b, c). For caption see p. 210.

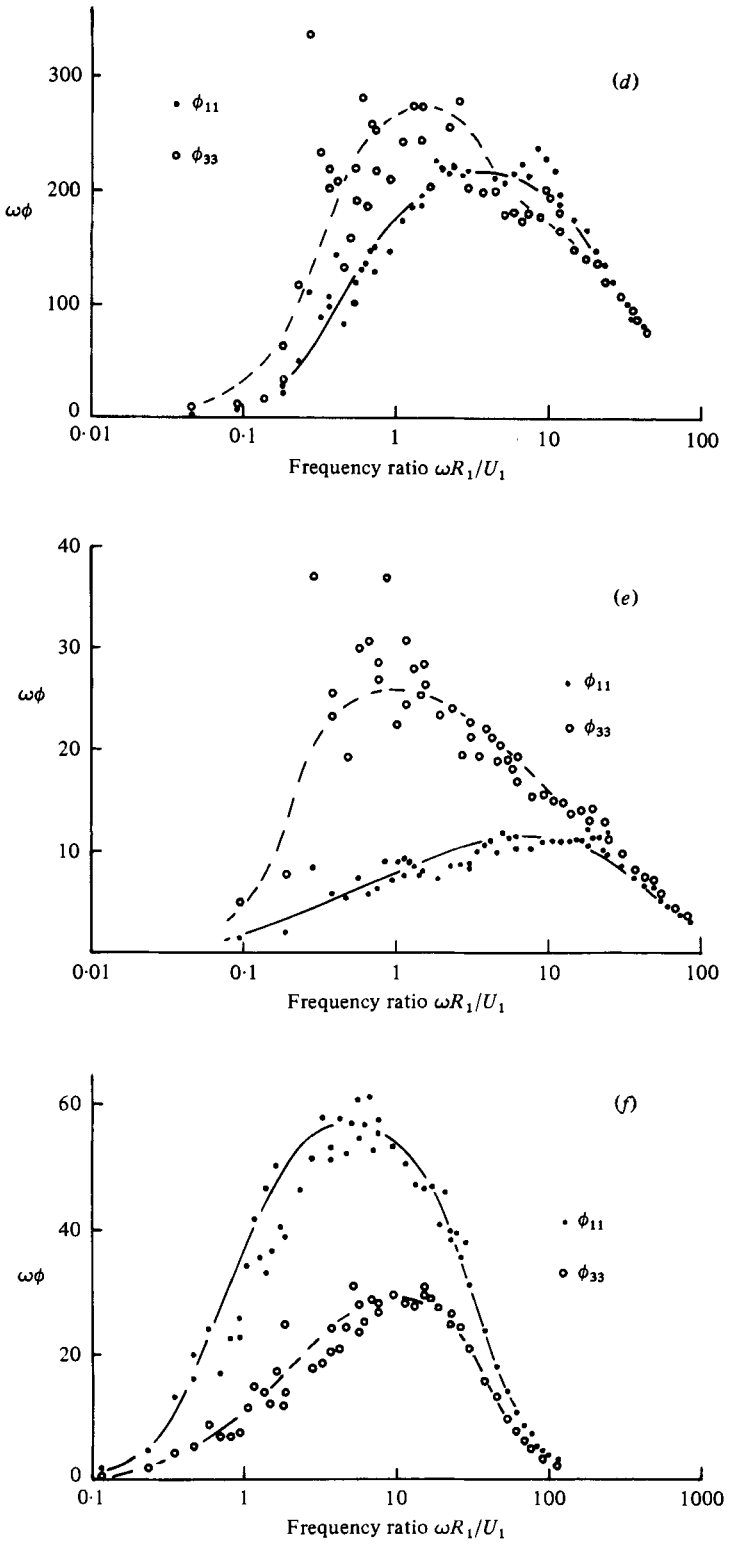

FIGURE 12(*d*, *e*, *f*). For caption see p. 210.

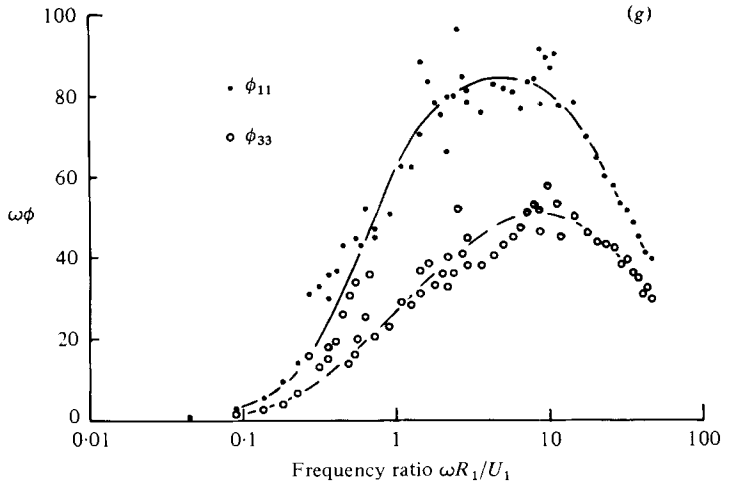

FIGURE 12. Spectra of the irregular, non-toroidal motion near the flow centre and near the inner cylinder. (*a*) ϕ_{11} and ϕ_{22} at $z/d = 0{\cdot}58$ for $Re = 20900$, $T^* = 75000$. (*b*) ϕ_{11} and ϕ_{33} at $z/d = 0{\cdot}64$ for $Re = 20900$, $T^* = 75000$. (*c*) ϕ_{11} and ϕ_{22} at $z/d = 0{\cdot}58$ for $Re = 52500$, $T^* = 472000$. (*d*) ϕ_{11} and ϕ_{33} at $z/d = 0{\cdot}64$ for $Re = 52500$, $T^* = 472000$. (*e*) ϕ_{11} and ϕ_{33} at $z/d = 0{\cdot}64$ for $Re = 97000$, $T^* = 1610000$. (*f*) ϕ_{11} and ϕ_{33} at $z/d = 0{\cdot}10$ for $Re = 20900$, $T^* = 75000$. (*g*) ϕ_{11} and ϕ_{33} at $z/d = 0{\cdot}10$ for $Re = 52500$, $T^* = 472000$. Note that the same scale is used for the two spectra on each graph, but the scale factor is arbitrary.

			Central flow ($r-R_1 = 28$ and 48 mm)						
		Ratios			Lower limit			Upper limit	
Re	u	v	w	u	v	w	u	v	w
21000	26	30	30	0·9	1·1	0·8	24	31	22
52000	60	92	65	0·65	0·47	0·4	37	42	24
98000	93	—	65	0·6	—	0·26	57	—	16
			Near inner cylinder ($r-R_1 = 8$ mm)						
Re	u	v	w	u	v	w	u	v	w
21000	28	73	25	0·74	0·4	0·4	34	52	44
52000	60	230	60	0·8	0·3	0·9	43	68	53
98000	73	—	102	1·2	—	0·6	84	—	63
			Near outer cylinder ($r-R_1 = 68$ mm)						
Re	u	v	w	u	v	w	u	v	w
21000	26	62	30	0·73	0·45	1·17	19	28	35
52000	77	—	66	0·6	—	0·7	34	37	45
98000	97	—	124	0·53	—	0·4	51	—	50

TABLE 2. Non-dimensional frequencies for spectral intensities of one-half the maximum value.

Equation (7.2) states that $\omega\phi$ is the convolution of $P(\ln T)$ with the component spectrum $\Phi(\ln \omega)$ on a logarithmic frequency scale, and so the (logarithmic) variance of the complete spectrum is the sum of the variances of the component spectrum and of the duration distribution function $P(\ln T)$. Assuming that squares of logarithms of ratios of half-intensities combine in the same way, knowledge of the ratio for the component spectrum would permit calculation of the ratio of the durations for half-intensity in the duration distribution. In table 3, ratios for the spread of duration have been calculated by assuming that the half-intensity ratio for the component

Central flow (for d = 28 mm and 48 mm)									
	Ratios			Lower limits			Upper limits		
Re	u	v	w	u	v	w	u	v	w
21000	11	11	11	1·45	1·45	1·45	16	16	16
52000	30	45	30	0·7	0·7	0·7	22	30	22
98000	50	—	35	0·8	—	0·35	40	—	11
Near inner cylinder (for d = 8 mm)									
	Ratios			Lower limits			Upper limits		
Re	u	v	w	u	v	w	u	v	w
21000	10	70	10	1·4	0·6	1·4	15	40	15
52000	30	130	30	1·1	0·4	1·1	32	55	32
98000	37	—	55	1·6	—	0·4	60	—	45
Near outer cylinder (for d = 68 mm)									
	Ratios			Lower limits			Upper limits		
Re	u	v	w	u	v	w	u	v	w
21000	10	30	10	1·5	0·6	1·5	15	20	15
52000	36	—	36	0·7	—	0·7	24	—	24
98000	52	—	70	0·7	—	0·5	38	—	35

TABLE 3. Limits to the distributions of passage duration of component eddies of the irregular motion, expressed as non-dimensional frequencies, which are themselves expressed as multiples of the rotation rate of the inner cylinder. For comparison, the non-dimensional orbital frequencies are: 0·32 in the central flow at d = 38 mm; 0·5 near the inner cylinder; 0·22 near the outer cylinder.

spectrum is ten, a value considered to be appropriate for component eddies of simple form (for a spectrum $\phi(x) = \exp(-\frac{1}{2}x^2)$, the ratio is 6·1 : 1; for $\phi(x) = (1+x^2)^{-1}$, it is 13·9 : 1). Corrected values for the upper and lower half-intensity frequencies are also listed.

Interpreting the 'corrected' half-intensity frequencies of table 3 as reciprocals of *twice* the durations of the longest and shortest components, and identifying convection velocities of the flow patterns with circumferential mean velocities, longitudinal scales of the irregular flow in the central region are found to change as follows.

(i) The ratio of maximum to minimum scale increases for each velocity component by a factor of 3 to 4 as the Reynolds number increases from 21000 to 52000. At the Reynolds number of 98000, the ratio for the circumferential component has increased by a further factor of 1·5, but the ratio for the radial component remains nearly the same.

(ii) At the lowest rotation speed, the maximum scale is close to 100 mm for all three velocity components, increasing to 200 mm at the intermediate speed. (For comparison, the circumference is nearly 1·2 m and the flow gap 76 mm.) At the top speed, the scale for the radial component has increased to 400 mm, but that of the circumferential component is unchanged (but see below).

(iii) Over the range of rotation speeds, the minimum scale of the circumferential component decreases from 10 mm to 8 mm to 4 mm, while the scale of the radial component changes very little, from 10 mm to 8 mm to 11 mm.

At the upper Reynolds number of 98000 ($T^* = 1{\cdot}64 \times 10^6$), the spectra of the circumferential and radial velocity components ϕ_{11} and ϕ_{33} are decidedly asymmetric on the logarithmic plot. As can be seen from figure 12, the spectral intensities are of similar magnitude for non-dimensional frequencies more than 20, but ϕ_{11} is much smaller than ϕ_{33} for frequencies in the range 0·1–5, in ratios of $\frac{1}{3}$ to $\frac{1}{4}$. It appears that

radial velocities of the longer duration components are considerably greater than circumferential velocities, and that the motion is predominantly in the yOz-plane.

The dissimilarity in shape between the two spectra for the upper Reynolds number has the effect of biasing the half-intensity frequencies in opposite directions, and the difference in maximum and minimum scales at that Reynolds number is more due to the biasing than to a real difference.

8. Discussion of results

Couette flow differs strongly from nearly unidirectional flows such as wakes, jets and channel flows in that flow structure changes very appreciably over a range of comparatively large Reynolds number. In contrast, the energy-containing motion of unidirectional flows is nearly statistically similar for all Reynolds numbers more than some five times the critical. The most obvious structural change is the decrease in the fractional energy of the toroidal motion, from over one-half to less than one-twentieth as the Reynolds number increases from one hundred to one thousand times the critical value, with accompanying changes in the spectra of the velocity fluctuations.

In Couette flow with the outer cylinder stationary, energy transfer from the mean flow to the fluctuations can occur by two very different kinds of instability. The mechanism of the first kind of instability resembles in many respects the Bénard instability in fluid heated from below in a gravitational field, and may be described as 'convective' instability. It favours the generation of roller eddies elongated in the flow direction, such as the toroidal eddies of the initial instability. The second kind, 'inertial' instability, occurs in channel flow between parallel walls, and usually leads directly to the formation of turbulent patches and bursts. In Couette flows with not too small ratios of gap to radius, the initial instability of the laminar flow is convective, occurring at a Reynolds number perhaps one-twentieth of that for the inertial transition in parallel flow, and, even when the flow becomes irregular, energy transfer to the fluctuations is by the convective mechanism.

The relative strengths of the two modes of instability is associated with the value of the curvature parameter, $\alpha = (U/r)/(dU/dr)$, the ratio of the flow angular velocity, on which the convective instability depends, to the velocity gradient, which is the energy source for the inertial instability. At large Reynolds numbers, most of the variation of mean velocity is within the thin wall layers whose thicknesses decrease steadily with increase of speed. It follows that, deep within them, values of the curvature parameter become small, and that, at sufficiently large Reynolds numbers, the local motion will be relatively unaffected by flow rotation and may develop inertial modes of energy transfer similar to those for plane flow. From consideration of upper bounds to the flow properties, Nickerson (1969) came to a similar conclusion and estimated that the change would occur at Reynolds numbers over 10^4.

If inertial effects are dominant close to the walls, each wall layer should consist of a viscous region of nearly uniform velocity gradient, an 'inertial' layer of turbulent flow similar to that on plane surfaces, and an outer transition layer in which curvature becomes important and angular momentum rapidly approaches the constant central value. The two outer regions are similar in properties to those in plane boundary layers with upward heat flux. Below a height proportional to the Monin–Obukhov length, the flow is little affected by buoyancy forces, and the distributions of velocity and temperature are logarithmic. Above that height, velocity and temperature appoach constant values. In Couette flow, the analogue of the Monin–Obukhov length is $G^{\frac{1}{2}}/2k\,U_{\mathrm{m}}$, where U_{m} is the velocity just outside the layer.

Re	$U_1R_1/G^{\frac{1}{2}}$	$G^{\frac{1}{2}}/\nu$	z_c^*	α_c	Outer α_{50}	Inner α_{50}
10000	25·3	790	30	(−0·26)	(−0·36)	(−0·30)
20000	27·6	1450	47	(−0·23)	(−0·20)	(−0·20)
50000	30·9	3230	94	−0·203	−0·088	−0·108
100000	33·7	5930	167	−0·197	−0·048	−0·080
200000	36·8	10870	312	−0·201	−0·026	−0·043

TABLE 4. Curvature parameters in a layer with logarithmic distribution of velocity. It has been assumed that $G/(U_1R_1)^2$ is proportional to $Re^{-\frac{1}{4}}$, with a value of $11{\cdot}0 \times 10^{-4}$ for $Re = 4{\cdot}06 \times 10^4$. The constants of the logarithmic velocity distribution are taken to be $k = 0{\cdot}41$, $A = 1{\cdot}8$. The values of α are for the (extrapolated) edge of the wall layers, and for the positions of $z^* = 50$ on the outer and inner layers. Bracketed values have no physical meaning since the calculated value of z_c^* is too small for a logarithmic distribution.

To assess the likelihood of inertial flow, assume that the velocity distribution outside the viscous layer is logarithmic, terminating where the calculated velocity becomes equal to the velocity just outside the layer, i.e.

$$\left.\begin{aligned} U &= \frac{\tau_2^{\frac{1}{2}}}{k}(\ln z^* + A) \quad \text{(outer cylinder)}, \\ U &= U_1 - \frac{\tau_2^{\frac{1}{2}}}{k}(\ln z^* + A) \quad \text{(inner cylinder)} \end{aligned}\right\} \tag{8.1}$$

in each case, for z^* less than z_c^*, where

$$z_c^* = \exp\left(\frac{\frac{1}{2}kU_1R_1}{G^{\frac{1}{2}}} - A\right). \tag{8.2}$$

Then values of the curvature parameter are calculated as

$$\left.\begin{aligned} \alpha &= -\frac{\nu}{G^{\frac{1}{2}}} z^*(\ln z^* + A) \quad \text{(outer cylinder)} \\ \alpha &= -\frac{\nu}{G^{\frac{1}{2}}} z^*\left(\frac{kU_1R_1}{G^{\frac{1}{2}}} - \ln z^* - A\right) \quad \text{(inner cylinder)} \end{aligned}\right\} \tag{8.3}$$

At the limits of the logarithmic profiles, the value is

$$\alpha_c = -\left(\frac{\frac{1}{2}k\nu}{G^{\frac{1}{2}}}\right)\left(\frac{U_1R_1}{G^{\frac{1}{2}}}\right) z_c^*. \tag{8.4}$$

Table 4 lists for a range of Reynolds numbers, (*a*) values of z_c^* and α_c, specifying the position of the layer limit and the curvature parameter there, and (*b*) values of the curvature parameter at $z^* = 50$ in each layer. If z_c^* is less than fifty, no significant region of logarithmic variation of velocity can exist, a condition that excludes any flow of Reynolds number less than 20000. At $z^* = 50$, the curvature parameter might be considered as becoming small for Reynolds numbers above 50000, sufficiently so to make plausible existence of a region of turbulent motion similar to that on a plane wall.

Values of the friction coefficient $G/(U_1R_1)^2$ used in compiling the table assume a variation as the $-\frac{1}{4}$ power of the Reynolds number. Such a variation is consistent with measured velocity gradients in the viscous regions, but the constancy of the tabulated values of α_c indicates that almost the same values of the friction coefficient for Reynolds numbers over 40000 would be obtained by assuming a constant value of $\alpha_c = -0{\cdot}20$.

In the real flow there is a transition layer, extending from where a logarithmic distribution of velocity implies a curvature parameter of significant magnitude and merging into the central region of constant angular momentum. For a Reynolds number of 50000, the variation of angular momentum between $z^* = 50$ and the central flow is hardly 5% of the total variation in the wall layer, and it is difficult to distinguish the transition layer from the inertial layer.

For Reynolds numbers less than about 20000, curvature affects the whole of the flow, and transfer of angular momentum from the viscous layer to the central region must be by eddies whose motion is strongly constrained by flow curvature. The photographs of Barcilon *et al.* (1979), taken in flows of Reynolds numbers up to 22000 (a Taylor-number ratio of 80000), show, in addition to the large-scale toroidal eddies, long circumferential streaks, identified by them as the result of Görtler vortices similar to those found in boundary layers on concave surfaces. Diameters of the vortices are comparable to the thickness of the wall layer, and they transfer angular momentum to the central flow sufficiently smoothly not to disrupt the toroidal eddies.

With increase of Reynolds number from 30000 to 80000, the peripheral coherence of the toroidal eddies becomes less and they either disappear into fully irregular, turbulent flow or, more probably, become too fragmented or distorted to be easily distinguishable. That they exist in fragmented form is suggested by comparison of spectra taken near the flow centre for Reynolds numbers of 20900 and 97000 (figures 12*b*, *e*). At the lower Reynolds number, spectra of the radial and circumferential velocity components are of similar form, with a lower limit at non-dimensional frequency near one and comparable intensities. At the higher Reynolds number, the lower frequency limit of the circumferential spectrum is hardly changed, but the radial spectrum extends to about 0·2 and, over a range of frequencies from 0·2 to 1·0, its intensities are greater in ratios of three or four to one. The regular toroids have, near the flow centre, velocity fluctuations almost entirely in the radial direction, and so the spectra are consistent with the presence of toroids of lengths ranging from about one-half of the flow perimeter to something comparable to the flow width.

A possible reason for the loss of regularity of the toroidal eddies is that the transfer of momentum across the wall layers is no longer by Görtler vortices elongated in the stream direction. If the motion deep within the layers now resembles turbulent flow on a plane wall, most of the transfer will be irregular, 'bursting' motions without extensive coherence in either the circumferential or axial directions, and the smooth boundary conditions necessary for formation of highly regular toroids no longer exist.

Another indication that the flow is changing in character is the decrease in magnitude of the overshoots in the distributions of angular momentum (figure 1*a*). The decrease in magnitude runs nearly parallel with the decrease in the fractional intensity of the toroidal eddies (figure 11). It is likely that the overshoots are caused by transfer of angular momentum from one wall layer directly to the other by toroidal eddies spanning the entire flow, and their disappearance would indicate that undisturbed transfer is less common at the higher Reynolds numbers. Without extensive measurements of velocity correlations, the radial extents of the toroidal fragments is uncertain, but the reduction of overshoot suggests that at least a proportion of them span only part of the flow width.

We review some of the results and conclusions.

(i) For Reynolds numbers less than 40000 (Taylor-number ratios less than 250000) the central flow is dominated by regular toroidal eddies, equally spaced along the cylinder axis and with motion nearly confined to axial planes.

(ii) For Reynolds numbers over 40000 the central motion becomes increasingly

irregular. Spectrum measurements indicate that much of the large-scale motion may consist of finite sections of toroidal eddies, of lengths from one or two flow widths to half the flow perimeter.

(iii) Over the same range of Reynolds number, regions appear in the wall layers within which the curvature parameter is moderately small, and distributions of mean velocity resemble closely the universal distribution for turbulent flow over a plane surface.

(iv) The transition region between the central flow of constant angular momentum and the outer limit of logarithmic variation is too limited in extent to be easily distinguishable. If the logarithmic profile is extrapolated to the central flow, the central angular momentum is attained for a (calculated) curvature parameter of $-0{\cdot}20$.

(v) The overshoots in the distributions of angular momentum diminish with Reynolds number, possibly because of reduced radial extent of eddies in the central flow.

(vi) Theoretical models for turbulent flow at high Reynolds numbers have been proposed by Landau (Landau & Lifshitz 1959) and by Malkus (1954, 1956), each suggesting that the flow may be treated as the superposition of normal modes of the stability equation. The inferred reduction in radial extent of the roller eddies in the central flow lends some support to the models.

Appendix. The analogy between Couette and stratified flows

In steady-state Couette flow between concentric cylinders, the equations for angular momentum flux, for balance of mean-square angular momentum fluctuation, and for balance of the kinetic energy of the radial and axial velocity components are

$$\left.\begin{aligned} \overline{uw}r^2 - \nu r^3 \frac{d}{dr}\left(\frac{U}{r}\right) &= G, \\ \frac{\overline{uw}}{r}\frac{d}{dr}(Ur) + \frac{1}{r}\frac{d}{dr}(\tfrac{1}{2}\overline{u^2 w}r) + \frac{\overline{u}}{r}\overline{\frac{\partial p}{\partial \theta}} &= \nu\overline{u\nabla^2 u}, \\ \frac{1}{r}\frac{d}{dr}(\overline{pw}r + \tfrac{1}{2}\overline{(v^2+w^2)w}r) &= \frac{2U}{r}\overline{uw} - \frac{\overline{u}}{r}\overline{\frac{\partial p}{\partial \theta}} + \nu(\overline{v\nabla^2 v} + \overline{w\nabla^2 w}). \end{aligned}\right\} \quad \text{(A 1)}$$

They may be compared with the equations for buoyancy flux, for balance of mean square buoyancy fluctuations, and for balance of turbulent kinetic energy in steady Bénard convection between parallel horizontal planes:

$$\left.\begin{aligned} \alpha\overline{\theta w} - \alpha k\frac{dT}{dz} &= \alpha Q, \\ \alpha\overline{\theta w}\frac{dT}{dz} + \alpha\frac{d}{dz}(\tfrac{1}{2}\overline{\theta^2 w}) &= \alpha k\overline{\theta\nabla^2\theta}, \\ \frac{d}{dz}(\overline{pw} + \tfrac{1}{2}\overline{(u^2+v^2+w^2)w}) &= \alpha g\overline{\theta w} + \nu(\overline{u\nabla^2 u} + \overline{v\nabla^2 v} + w\overline{\nabla^2 w}), \end{aligned}\right\} \quad \text{(A 2)}$$

where α is the coefficient of thermal expansion, T is the mean temperature at height z, θ is the temperature fluctuation, Q is the constant thermometric heat flux, and w is the velocity fluctuation in the vertical z-direction.

Comparison of the two sets of equations suggests an analogy between the two flows, the angular momentum flux $\overline{uw}r$, analogous to the buoyancy flux $\alpha\overline{\theta w}$, $2U/r^2$ to g, and $d(Ur)/dr$ to $\alpha dT/dz$. Some necessary conditions for validity are:

(i) that circumferential pressure gradients, $\partial p/\partial\theta$, are small:

(ii) that circumferential velocity fluctuations are distinct in function from the axial and radial fluctuations, which compare with the three-dimensional motion of the Bénard convection;

(iii) that radial variation of $2U/r^2$ can be ignored;

(iv) that the range of r is small.

Then the functional form of the variation of angular momentum near one cylinder of a Couette flow may be found using arguments similar to those for Bénard convection.

If variation of Ur is confined to thin wall layers, each layer may be considered as uninfluenced by the presence of the other, and the radial and axial motion within it is determined by the angular-momentum flux, $\overline{uw}r = G/r$, by $2U/r^2$, and by the fluid viscosity. The analogue of gravity, $2U/r^2$, is far from constant, but transfer of energy to the radial–axial motion is appreciable only in the outer region, where the total variation is about 25 %. A typical or effective value is $2U_m/r^2$, where U_m is the velocity on the outer edge of the wall layer.

On these assumptions, the velocity scale for the radial-axial motion is

$$u_0 = \left(\frac{2\nu G U_m}{r^3}\right)^{\frac{1}{4}}, \tag{A 3}$$

and the lengthscale is

$$z_0 = \frac{\nu^{\frac{3}{4}} r^{\frac{3}{4}}}{(2GU_m)^{\frac{1}{4}}}. \tag{A 4}$$

Angular-momentum fluctuations ur are transferred by velocity fluctuations of magnitude u_0, and so the scale of angular momentum variation is

$$p_0 = \frac{\overline{uw}r}{u_0} = \frac{G^{\frac{3}{4}}}{(2\nu U_m r)^{\frac{1}{4}}}. \tag{A 5}$$

The distribution of mean angular momentum near a cylinder of radius R_w moving with peripheral velocity U_w will be of the form

$$Ur - U_w R_w = p_0 f(z/z_0) \tag{A 6}$$

where necessarily $f(\eta) = \eta$ for small values of $\eta = z/z_0$ within the viscous layer. The total variation across the wall layer is

$$(Ur)_{\text{central}} - U_w R_w = C p_0. \tag{A 7}$$

Since Ur is almost constant outside the wall layers, p_0 has the same value in each layer, and the central value of the mean angular momentum is the average of the wall values.

For the experimental arrangement with the outer cylinder stationary, the central value of angular momentum is $\frac{1}{2}U_1 R_1$, and the relation between torque coefficient $G/U_1^2 R_1^2$ and Reynolds number $U_1 R_1/\nu$ is

$$\frac{G}{U_1^2 R_1^2} = (2C)^{-\frac{4}{3}} \left(\frac{U_1 R_1}{\nu}\right)^{-\frac{1}{3}}. \tag{A 8}$$

For $U_1 R_1/\nu = 81\,300$, the torque coefficient is $1{\cdot}1 \times 10^{-3}$, and the 'constant' C is calculated to be 4·9, to be compared with values near 3·5 in Bénard convection. Using the estimated value for the lowest speed (1·7 m/s), C is found to be 4·45.

REFERENCES

BARCILON, A., BRINDLEY, J., LESSEN, M. & MOBBS, F. R. 1979 *J. Fluid Mech.* **94**, 453.

COLES, D. 1965 *J. Fluid Mech.* **21**, 385.

DI PRIMA, R. C. & SWINNEY, H. L. 1981 In *Hydrodynamic Instabilities and the Transition to Turbulence* (ed. H. L. Swinney & J. P. Gollub), p. 139. Springer.

GOLLUB, J. P. & SWINNEY, H. L. 1975 *Phys. Rev. Lett.* **35**, 927.

HOWARD, L. N. 1963 *J. Fluid Mech.* **17**, 405.

KOSCHMIEDER, E. L. 1979 *J. Fluid Mech.* **93**, 515.

LANDAU, L. D. & LIFSHITZ, E. M. 1959 *Fluid Mechanics.* Pergamon.

MALKUS, W. V. R. 1954 *Proc. R. Soc. Lond.* A **225**, 185.

MALKUS, W. V. R. 1956 *J. Fluid Mech.* **1**, 521.

NAKAMURA, I., YAMASHITA, S., WATANABE, T. & SAWAKI, Y. 1981 In *Proc. 3rd Symp. on Turbulent Flows; University of California, Davis.*

NICKERSON, E. C. 1969 *J. Fluid Mech.* **38**, 807.

ROBERTS, P. H. 1965 *Proc. R. Soc. Lond.* A **283**, 550.

TAYLOR, G. I. 1923 *Phil. Trans. R. Soc. Lond.* A **223**, 289.

TAYLOR, G. I. 1936 *Proc. R. Soc. Lond.* A **158**, 565.

VAN ATTA, C. 1966 *J. Fluid Mech.* **25**, 495.

WANG, A. K. M. & GELHAR, L. W. 1970 *M.I.T. Dept Civil Engng Rep.* no. 132.